Enabling Techniques for Biomedical Research

Ashley M. Dostie

A dissertation
submitted in partial fulfillment of the
requirements for the degree of

Doctor of Philosophy

University of Washington
2022

Reading Committee:
Ashleigh B. Theberge, Chair
Alshakim Nelson
Robert Synovec

Program Authorized to Offer Degree:
Chemistry

University of Washington

Abstract

Enabling techniques for biomedical research

Ashley M. Dostie

Chair of the Supervisory Committee:
Assistant Professor Ashleigh B. Theberge
Department of Chemistry

This dissertation discusses a variety of elements including the study of open microfluidic capillary systems, the generation of hydrogels with lumens and cell culture using these systems, and an UW IRB-approved study involving the immune response to COVID-19. Chapter 1 provides an introduction to open microfluidics capillary systems as well as cell culture using hydrogels. Chapter 2 investigates the effect of combining two types of capillary pumps within an open microfluidic devices on multiple solvent types. Chapter 3 discusses multiple methods of making hydrogel lumens, including culturing endothelial cells on the luminal wall and culturing smooth muscle cells within a hydrogel ring. The first method involves extrusion of hydrogel tubes while the second method discuses a device used to fabricate hydrogel rings. Chapter 4 introduces an ongoing COVID-19 pre-symptomatic study. The study design is presented along with initial demographics data for participants and feedback on study kit usability.

TABLE OF CONTENTS

LIST OF FIGURES

ACKNOWLEDGEMENTS

Thank you to Ashleigh Theberge for your guidance and generosity while letting me pursue a doctorate within your lab. I truly could not have asked for a better mentor or PI. I was lucky enough to help you start the lab and watch your lab grow from 2 graduate students and 3 undergraduates to where it is now. I find that I am at a loss for words to describe how much I value your mentorship in chemistry, in lab, in teaching, and in life. Thank you for helping me grow to who I am today.

Thank you to Alshakim Nelson and Robert Synovec who have both provided wisdom surrounding both my dissertation and life as a scientist. I have very much enjoyed working with both of you over the years and am grateful for all of the advice you have given me.

To everyone else - I could not have done this without many people in my life; too many to name. Thank you to all of you; friends, family, everyone.

Chapter 1. INTRODUCTION

1.1 OPEN MICROFLUIDICS

Reproduced in part from E. Berthier, A. M. Dostie,* U. N. Lee, J. Berthier, A. B. Theberge,§ "Open microfluidic capillary systems." Anal. Chem., 2019.* ***91****, 8739.*
** Equal contribution*

In the constantly evolving field of microfluidics, a recent branch of study focuses open microfluidics. In a traditional closed microfluidic system the liquid is fully enclosed on each side; in an open microfluidic system, at least one 'wall' is removed resulting in an air-liquid interface. Open microfluidics can use capillary forces to drive flow, as opposed to external actuation such as fluid pumps. Open microfluidic capillary systems have emerged as powerful tools with broad applications demonstrated by laboratories around the world in cell culture, sample collection and preparation, metabolite and protein assays, and interfacial chemistry. Different types of open microfluidic capillary configurations are possible, ranging from simple channels devoid of a ceiling, to open 'rails' in which fluid flows along two ridges and is exposed to two air-liquid interfaces, to paper- and thread-based devices in which fluid travels along patterned conditions for flow in open microfluidic capillary systems can broadly be determined by the 'spontaneous capillary flow' equation which relates the ability of a fluid to flow in an open channel with the channel wettability (for a given material and liquid of interest) and channel geometry.

1.1.1 *Advantages and Disadvantages of Open Microfluidic Capillary Systems*

The configuration of open devices, compared to closed or semi-open microfluidic systems, provides numerous advantages including: simplification of manufacturing techniques and surface modification; significant improvement in device reliability through elimination of failures

resulting from bubble formation; and the unique ability to access the fluid at any point in the channel in order to input or sample fluid.

One potential disadvantage of working with an open device includes the potential for evaporation of any liquids in the system; this can be exacerbated by the use of volatile solvents. There are methods to mitigate evaporation in open devices, including surrounding a device with sacrificial droplets of water[1] or placing the system in a secondary humidified container. Another disadvantage is the limited range of pressures that can be generated within an open system. Adjusting channel dimensions can change the pressures within a system, but this will also change other factors such as fluidic resistance.

1.1.2 *Capillary Pumps*

Flow in open microfluidic systems relies on the capillary advance of the fluid in the channel and is intrinsically limited in volume and in duration. Further, as the length of the channel increases, the flow rate decreases. The duration and stability of the pumping can be increased using capillary pumping techniques. Capillary pumping techniques can be grouped in two categories: the first relies on using a wicking material that can absorb a large volume of fluid (such as a cotton or paper pad), while the second relies on multiplexing a large number of discrete channels to allow more volume of fluid to flow through the system while each channel remains short in length.[2,3] An example of this could be the addition of many capillary tubes or a bundle of fibers to the end of an open channel, increasing the capillary force and thus the flow.

1.2 Cell Culture in Hydrogels

Scientist have worked with many materials to culture cells, including expanding from traditional two-dimensional (2D) cultures on plastic surfaces to culturing cells on or within hydrogels,

creating a three-dimensional (3D) environment. Mammalian cells experience a three-dimensional space within the human body, surrounded by varying extracellular matrix components and cell types that are determined by the location within the body and the function of that tissue. Attempts to make cultures more biomimetic by incorporation of relevant hydrogels, multi-culture of different cell types, or generation of specific architectures such as tubular structures have resulted in changes in cell behavior that more closely replicate what is observed *in vivo.*[4,5] The ideal disease model would closely recapitulate the microenvironment for cells from a specific tissue.

A lumen is the cavity within a tube or tubular organ; lumen structures exist in several different tissue types, and numerous experimental methods have incorporated the fabrication of lumen.[4,6] In this work, two different methods of generating a lumen structure for cell culture experiments will be presented.

1.3 REFERENCES

1. E. Berthier, J. Warrick, H. Yu, D. J. Beebe, *Lab Chip*, 2008, **8**, 852
2. J. Berthier, *The Physics of Microdroplets*, Wiley, Hoboken, NJ, USA 2012
3. M. Zimmermann, P. Hunziker, E. Delamarche, *Microfluid Nanofluid*, 2008, **5**, 395
4. L. L. Bischel, et. al., "The importance of being a lumen." *FASEB*, 2014. **28**, 4583
5. F. Pampaloni, E. G. Reynaud, E. H. Stelzer, "The third dimension bridges the gap between cell culture and live tissue." *Nat. Rev. Mol. Cell. Biol.*, 2007. **8**, 839
6. J. A. Jiménez-Torres, S. L. Peery, K. E. Sung, D. J. Beebe, "LumeNEXT: A practical method to pattern luminal structures in ECM gels." *Adv. Healthcare Mater.*, 2016. **5**, 198

Chapter 2. CAPILLARY PUMPING IN AN OPEN MICROFLUIDIC SYSTEM

Reproduced in part from J. J. Lee, J. Berthier,* A. M. Dostie, J. W. Khor, A. B. Theberge,§ E. Berthier, § "Enhanced capillary pumping using open-channel capillary trees with integrated paper pads." In review at* Sensors and Actuators B, ***2022***.
** Equal contribution*
§ Co-corresponding authors

Devices were designed by J. J. Lee and J. Berthier. Fabrication of devices and experiments were performed by J. J. Lee and A. M. Dostie. Experimental results were processed by J. J. Lee, A. M. Dostie, and J. W. Khor.

Abstract: The search for efficient capillary pumping has led to two main directions for investigation: first, assembly of capillary channels to provide high capillary pressures, and second, imbibition in absorbing fibers or paper pads. In the case of open microfluidics (i.e., channels where the top boundary of the fluid is in contact with air instead of a solid wall), the coupling between capillary channels and paper pads unites the two approaches and provides enhanced capillary pumping. In this work, we investigate the coupling of capillary trees—networks of channels mimicking the branches of a tree—with paper pads placed at the extremities of the channels, mimicking the small capillary networks of leaves. It is shown that high velocities and flow rates (18 mm^3/s or 30 µl/s for more than 30 seconds; >3.5 mm^3/s or 5 µl/s for more than 200 seconds) can be reached in the root channel, enabling higher sustained flow rates than are achievable with capillary trees alone.

2.1.1 *Overview*

Simple and autonomous microfluidic systems can be designed by use of capillary forces. In such systems, bulky active pumps[1,2] are not needed. However, a major drawback in a capillarity-based system is the decrease of the flow velocity—and the flow rate—with time. According to the Lucas-Washburn-Rideal (LWR) law, the decrease of the velocity is proportional to the inverse of the

square root of time.[3-5] To overcome this drawback, multiple capillary pump designs have been developed. These pumping systems can be networks of small channels where the capillary pressure is high, or matrices of fibers (often paper pads) with a high wicking power. These capillary pumps are placed behind the "region of interest" where the biological or chemical processes are performed and can be used in multiple applications including separation methods or sample processing.

Capillary trees for capillary pumping in closed (confined) channels have been developed.[6] Examples include triple tree line capillary pumps used for performing immunoassays,[7] and microstructures for simple and advanced capillary pumping.[8] On the other hand, it was shown that microporous and fibrous structures, such as paper pads, provide efficient pumping due to their high wicking power.[9-11]

In the realm of capillary-driven microfluidics, open systems are of special interest.[12-14] These systems remove at least one 'wall' of the microfluidic channel, often the top wall, providing easy access to the flowing liquid. We have previously found that a capillary tree can be used to maintain a high value of velocity in the root channel—the channel of interest for a given application—in open microfluidic devices.[15]

In this work, we show that these capillary tree channels can easily be connected to paper pads (mimicking the small capillary networks of leaves); this additive structure takes advantage of the pumping effect of the two systems, the capillary tree and the fibrous paper "leaves". The paper pads are placed in milled receptacles at the end of the branched channels. We used a geometric design of capillary trees where the root channel is successively divided in a cascade of daughter channels and the cross sections of the daughter channels are progressively decreased in a ratio of 0.85. A high flow rate in the root channel can be achieved and sustained with such designs (Figure 2.1).

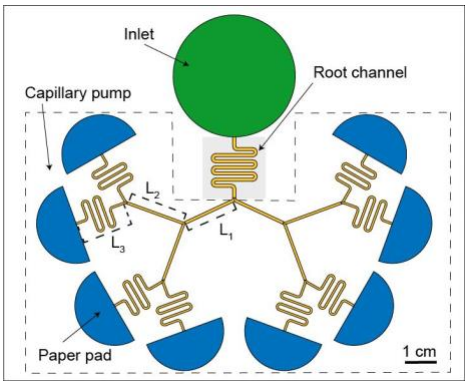

Figure 2.1. Diagram of an open channel microfluidic device utilizing a capillary tree channel and paper pads.

2.1.2 *Results*

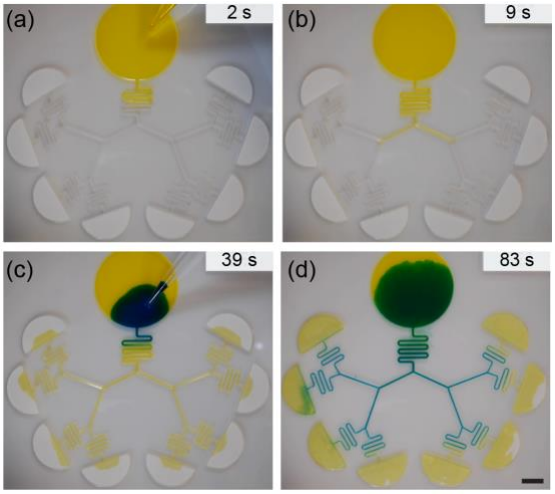

Figure 2.2. Still images of an open channel device filled with yellow and blue IPA solutions. (a) Yellow liquid is pipetted in the inlet of the open channel. (b) Progression of the yellow liquid in the root channel and capillary tree. (c) Blue liquid is pipetted in the inlet after the yellow liquid reached the paper pad. (d) Progression of blue liquid in the open channel. Scale bar is 1 cm.

Figure 2.2 shows the flow of fluid in a device that combines a capillary tree and paper pads. Experiments included the use of colored solutions of 20% IPA (v/v), 50% IPA (v/v), and nonanol. The experimentally determined travel distances and times are shown in Figure 2.3. In the paper pads, a good fit was found for capillary pressures of 5200 and 3000 Pa respectively. In the case of the 20% IPA solution (Fig. 2.3), root channel velocities of the order of 15-17 mm/s were obtained

for 30 seconds. In the case of the 50% IPA solution (Fig. 2.3), root channel velocities of the order of 7 mm/s were obtained for 60 seconds. The contact of the liquid with the pads is around 20 seconds for 20% IPA, 35 seconds for 50% IPA, and 95 s for nonanol (Fig. 2.3).

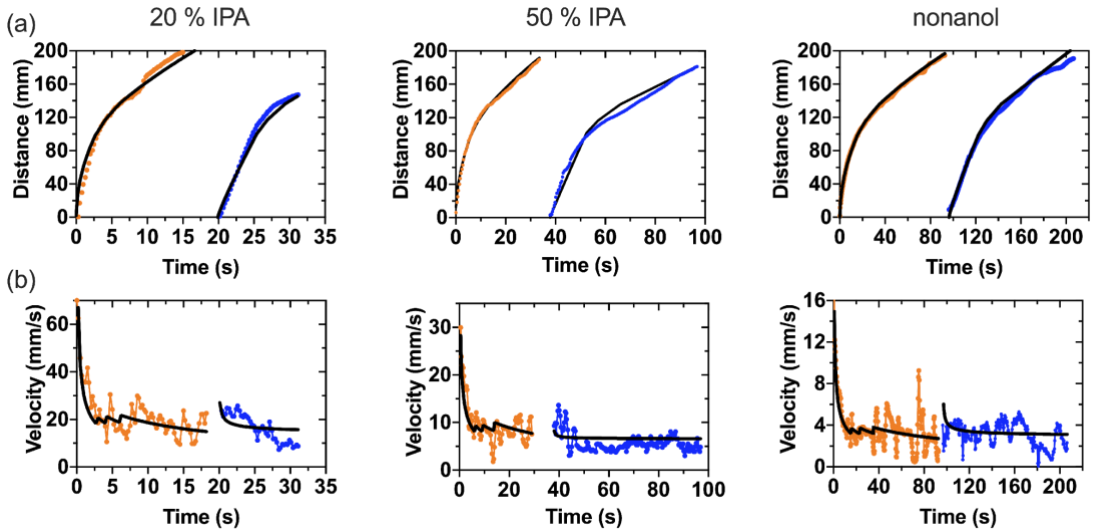

Fig. 2.3. Travel distance and velocity over time for 20% and 50% (v/v) IPA solution and nonanol solutions in an open channel capillary tree with paper pads. (a) Experimentally determined travel distances in the bifurcating capillary tree vs. time for the first phase of the flow (orange dots) and the second phase of the flow (blue dots) after the flow has reached the pads and blue colored solution has been added to the inlet. Travel distance was determined by measuring the distance of the fluid front in the device in the recorded videos. The black lines are the theoretical results. (b) Velocities in the root channel vs. time when the tip of the flow is in the capillary tree (orange dots) and in the paper pads (blue dots).

2.1.3 *Methods*

2.1.3.1 Fabrication of capillary tree channels

The device consists of winding channels (the root channel), a large inlet in which the liquid is introduced using a pipette, three levels of branches, and paper pads at the extremity of the last channel branches (Fig. 1). The widths and depths of the channels are homothetically reduced by a factor of 0.85 after each bifurcation. The turns in the winding channels do not affect the capillary flow in the absence of capillary filaments,[16] as the rounded bottom avoids the formation of filaments observed in channels of rectangular cross section.[17] The average friction length of the root channel is estimated to be $\underline{\lambda} \sim 259$ µm from our preceding work.[15,18]

The channels were designed using computer aided design (CAD) software (Solidworks 2017, Waltham, MA) and the design files were converted to G-code using computer aided manufacturing (CAM) software (Fusion 360). Channels were milled in poly(methyl methacrylate) (PMMA) sheets (3.175 mm thick, #8560K239; McMaster-Carr, Sante Fe Springs, CA). To create round bottom channels, endmills with a cutter diameter of 1/32" (TR-2-0312-BN) and 1/64" (TR-2-0150-BN) were used (Performance Micro Tool, Janesville, WI). The devices were fabricated via micromilling on a Datron Neo computer numerical control (CNC) mill (Datron, Germany). The channel bottom is estimated to have a few microns of roughness which is one magnitude below the roughness values that were observed by Lade et al.[19] that would produce fluctuations in velocity.

2.1.3.2 Paper pads

Whatman #1 paper was cut into half circle shapes using a Plotter cutter (Graphtec). The main characteristics of the paper pads are listed in the Supplemental Material Table SIII. The capillary pressure depends on the liquid that is used and the values are in alignment with the experimental results.

2.1.3.3 Solvents

The physical properties of the solvents are indicated in the Supplemental Material Table SI. To mitigate evaporation of the solvent, nonanol, which is a low volatile solvent (boiling is 213°C), was used. Nonanol has been colored with either Solvent Yellow 7 or with Solvent Green 3 (Sigma-Aldrich) at concentrations of 0.50 mg/mL and 1.43 mg/mL respectively. Aqueous isopropyl alcohol (IPA) was used at concentrations of 20% and 50% (v/v) and colored with 0.60 % yellow or 1.2 % blue food coloring. (McCormick). Note that the surface tension of aqueous IPA solutions

decreases with the concentration while the viscosity increases, but the capillary force ($\gamma\cos\theta$) stays nearly constant above a concentration of 20% (v/v).

2.1.3.4 Imaging

Videos of the progression of the flow of the solvent in the device were recorded using a Nikon-D5300 ultra-high resolution single lens reflective (SLR) camera. The location of the tip of the flow is pinpointed using MATLAB software.

2.1.4 *References*

1. L. Gervais, M. Hitzbleck, and E. Delamarche, *Capillary-Driven Multiparametric Microfluidic Chips for One-Step Immunoassays*, Biosens. Bioelectron. **27**, 64 (2011).
2. R. Safavieh and D. Juncker, *Capillarics: Pre-Programmed, Self-Powered Microfluidic Circuits Built from Capillary Elements*, Lab Chip **13**, 4180 (2013).
3. R. Lucas, *Ueber Das Zeitgesetz Des Kapillaren Aufstiegs von Flüssigkeiten*, Kolloid-Zeitschrift **23**, 15 (1918).
4. E. W. Washburn, *The Dynamics of Capillary Flow*, Phys. Rev. **17**, 273 (1921).
5. E. K. Rideal, *On the Flow of Liquids under Capillary Pressure*, Philos. Mag. Ser. 6 **44**, 1152 (1922).
6. A. Olanrewaju, M. Beaugrand, M. Yafia, and D. Juncker, *Capillary Microfluidics in Microchannels: From Microfluidic Networks to Capillaric Circuits*, Lab on a Chip.
7. M. Pla-Roca and D. Juncker, *PDMS Microfluidic Capillary Systems for Patterning Proteins on Surfaces and Performing Miniaturized Immunoassays.*, Methods Mol. Biol. **671**, 177 (2011).
8. M. Zimmermann, H. Schmid, P. Hunziker, and E. Delamarche, *Capillary Pumps for Autonomous Capillary Systems*, Lab Chip **7**, 119 (2007).
9. S. Mendez, E. M. Fenton, G. R. Gallegos, D. N. Petsev, S. S. Sibbett, H. A. Stone, Y. Zhang, and G. P. López, *Imbibition in Porous Membranes of Complex Shape: Quasi-Stationary Flow in Thin Rectangular Segments*, Langmuir **26**, 1380 (2010).
10. X. Wang, J. A. Hagen, and I. Papautsky, *Paper Pump for Passive and Programmable Transport*, Biomicrofluidics **7**, (2013).
11. T. Kokalj, Y. Park, M. Vencelj, M. Jenko, and L. P. Lee, *Self-Powered Imbibing Microfluidic Pump by Liquid Encapsulation: SIMPLE*, Lab Chip **14**, 4329 (2014).
12. J. Berthier, K. A. Brakke, and E. Berthier, *Open Microfluidics*, 1 (2016).
13. J. Berthier, E. Berthier, and A. B. Theberge, *Open-Channel Microfluidics: Fundamentals and Applications* (Morgan and Claypool Publishers, 2019).
14. E. Berthier, A. M. Dostie, U. N. Lee, J. Berthier, and A. B. Theberge, *Open Microfluidic Capillary Systems*, Analytical Chemistry.
15. J. J. Lee, J. Berthier, K. E. Kearney, E. Berthier, and A. B. Theberge, *Open-Channel Capillary Trees and Capillary Pumping*, Langmuir **36**, 12795 (2020).

16. J. Berthier, K. A. Brakke, D. Gosselin, F. Navarro, N. Belgacem, and D. Chaussy, *Spontaneous Capillary Flow in Curved, Open Microchannels*, Microfluid. Nanofluidics **20**, 1 (2016).
17. J. Berthier, K. A. Brakke, D. Gosselin, M. Huet, and E. Berthier, *Metastable Capillary Filaments in Rectangular Cross-Section Open Microchannels*, AIMS Biophys. **1**, 31 (2014).
18. J. J. Lee, J. Berthier, A. B. Theberge, and E. Berthier, *Capillary Flow in Open Microgrooves: Bifurcations and Networks*, Langmuir **35**, 10667 (2019).
19. R. K. Lade, E. J. Hippchen, C. W. Macosko, and L. F. Francis, *Dynamics of Capillary-Driven Flow in 3D Printed Open Microchannels*, Langmuir **33**, 2949 (2017).

Chapter 3. GENERATING HYDROGEL LUMENS

The content of this chapter will discuss two different methods of forming a hydrogel containing a lumen, as well as culturing of various cell types either on or within the hydrogels. The first part of this chapter will focus on using a casting method to create hydrogel rings that have smooth muscle cells embedded within the hydrogel, as well as adding endothelial cells to the lumen of the hydrogel rings. The second part of this chapter will discuss the addition of endothelial cells to the luminal wall of a hydrogel tube that was extruded through a 3D printed coaxial nozzle.

3.1 FREESTANDING HYDROGEL LUMENS FOR MODELING BLOOD VESSELS AND VASODILATION

Reproduced in part from A. M. Dostie, H. G. Lea,* U. N. Lee,* T. L. van Neel, E. Berthier, A. B. Theberge, "Freestanding hydrogel lumens for modeling blood vessels and vasodilation." In review at* SLAS Technology, ***2022***. *bioRxiv, https://doi.org /10.1101/2021.10.19.464875v1*.
** Equal contribution*

Abstract: Lumen structures exist throughout the human body, and the vessels of the circulatory system are essential for carrying nutrients and oxygen and regulating inflammation. Vasodilation, the widening of the blood vessel lumen, is important to the immune response as it increases blood flow to a site of inflammation, raises local temperature, and enables optimal immune system function. A common method for studying vasodilation uses excised vessels from animals; major drawbacks include heterogeneity in vessel shape and size, time-consuming procedures, sacrificing animals, and differences between animal and human biology. We have developed a simple, user-friendly *in vitro* method to form freestanding cell-laden hydrogel rings from collagen and quantitatively measure the effects of vasodilators on ring size. The hydrogel rings are composed of collagen I and can be laden with human vascular smooth muscle cells, a major cellular and structural component of blood vessels, or lined with endothelial cells in the lumen. The methods

presented include a 3D printed device (which is amenable to future fabrication by injection molding) and commercially available components (e.g., Teflon tubing or a syringe) to form hydrogel rings between 2.6-4.6 mm outer diameter and 0.79-1.0 mm inner diameter. Here we demonstrate a significant difference in ring area in the presence of a known vasodilator, fasudil (p<0.0001). Our method is easy to implement and provides a foundation for a medium-throughput solution to generating vessel model structures for future investigations of the fundamental mechanisms of vasodilation (e.g., studying uncharacterized endogenous molecules that may have vasoactivity) and testing vasoactive drugs.

3.1.1 *Introduction*

Lumen structures exist throughout the body including in the glandular organs such as the breast and prostate, and blood vessels of the circulatory system. Vasodilation, the widening of the blood vessel lumen, is important to the immune response as it increases blood flow to a site of inflammation, raises local temperature, and enables optimal immune system function.[1] Over the last two decades, tissue engineers and cell biologists have been working towards performing cell culture experiments in a three-dimensional environment, as opposed to two-dimensional culture.[2-4] It is well accepted that in the human body, cells are encapsulated in a 3D environment (extracellular matrix, ECM) and receive signals very differently than they would in a 2D polystyrene culture plate. Incorporation of relevant hydrogels, multi-culture of different cell types, or generation of specific architectures, such as tubular structures, have resulted in changes in cell behavior that more closely recapitulate *in vivo* cell function and morphology.[5, 6] Such observations have been increasingly helpful in drug discovery and tissue engineering due to increased cell to cell contact, cell communication, and cell-ECM interactions.[3] Current methods for studying vasodilation and constriction involve time-consuming *ex vivo* methods utilizing blood vessels

excised from animals (e.g., rabbit and rodent models), and simplified *in vitro* methods that capture a portion of the biological response.[7-10] While excised animal vessels are valuable in understanding cell signaling in an *ex vivo* environment, procedures are time intensive, requiring processing of the excised tissue and then almost immediate testing of samples; additionally, the responses observed in these excised vessels may not be representative of a response in human tissue.[11] An innovative model system is needed that is (1) simple to use and multiplex, enabling rapid adoption by biology laboratories, (2) incorporates multiple human cell types, and (3) can quantify the degree of dilation. To offer an alternative to animal methods and clinical trials in humans,[12-14] several groups have recently developed *in vitro* assays with primary human smooth muscle cells to study the effects of vasoactive compounds.[11, 15-18] Alford *et al.* created what they called 'muscular thin filament', or MTFs, which are strips of polydimethylsiloxane (PDMS) with adhered vascular smooth muscle cells.[15] The MTFs were imaged and analyzed, measuring constriction or dilation by curvature of the MTF.[15, 17, 19] Alternatively, several groups have performed vasoactivity tests on tissue engineered blood vessels (TEBVs) as part of characterization of TEBVs to be used for drug testing[16] or to be potentially implanted as vascular grafts.[18] Recently, Tseng *et al.* developed a platform to study vasoactivity of vascular smooth muscle cells that were 3D printed into a ring configuration that fit within the well of a 96-well plate.[11] Other well-based methods have been created that enable cells to settle and self-assemble into a ring formation.[20, 21] We sought to add to this body of work by developing a user-friendly method for generating blood vessel mimics that require only commercially available supplies and simple parts produced with an inexpensive resin 3D printer. Additionally, the device can be scaled up by injection molding in polystyrene, a common cell culture material.[22]

Here, we present a modular casting method to form a 3D hydrogel structure with a lumen (i.e., a ring) that is embedded with smooth muscle cells. The method is user friendly and amenable to medium-throughput experiments (~100 rings per day). These hydrogel rings are 2.6-4.6 mm in outer diameter, 0.79-1.0 mm in inner diameter, and are free-standing and transferable between well plates. The lack of attachment to any surface enables the hydrogel to be remodeled by the cells; thus, the addition of vasoactive compounds results in a visible and quantifiable readout. Our method enables the use of smooth muscle cells embedded in the hydrogel and endothelial cells in the lining of the lumen. Our method has the potential to be developed further and used to assay potential drug candidates to reduce harmful vasodilation in patients with various inflammatory diseases (e.g., asthma, rheumatoid arthritis, Raynaud's syndrome).

3.1.2 *Results*

Our goal was to develop a user-friendly protocol for producing cell-laden hydrogel rings that can be used for medium-throughput biological and drug screening experiments. Lumen structures are commonplace in the human body; our area of focus in this work was modeling blood vessels to study vasodilation. Here we present two casting methods to produce cell-laden hydrogel rings; our methods are easy to implement with 3D printed components and low-cost commercially available materials (e.g., Teflon tubing).

To use cell-laden hydrogel rings in vasoactivity experiments, it is important that the hydrogel is not attached to stiff materials that may prevent hydrogel deformation (i.e., dilation or constriction); therefore, our approach was to cast hydrogels using an easily removable mold. We used a simple 3D printed design and Teflon tubing to mold precursor hydrogel solution into a ring that could be removed and placed in a standard 96-well plate. Current 3D printed molds consist of 6 posts per device, enabling the generation of 6 hydrogel rings per mold. It is feasible to make ~100 rings per

day with each rack taking ~10 minutes total for assembly and loading of hydrogel. Incubation time varies on the hydrogel used (1 h for collagen). Other methods that utilize specialized assemblies to hold or rotate the rings during incubation limit the throughput of hydrogel ring structures to approximately <10 per experiment. Additionally, testing vasodilation with *ex vivo* vessels from mice or rabbits and wire myography only enables the measurement of 1-4 vessels at a time.[23] A PDMS spacer was applied to the device, and Teflon tubing was added onto each post (Figure 3.1Aii). The PDMS spacer holds up the Teflon tubing and enables the tubing to slide down the post and unmold the hydrogel ring when the spacer is removed. F127 (a polyethylene glycol (PEG)-based hydrogel) was added to seal any gaps between the tubing and the 3D printed post. We chose F127 as a sacrificial layer because it is not toxic to cells and easily dissolves once placed in a liquid such as cell culture media or phosphate buffered saline (PBS). After the F127 gelled, collagen I was added to form the ring. Once the collagen I polymerized the PDMS spacer was removed and the device was placed in PBS. The tubing was pushed down into the gap created by the removal of the PDMS spacer to reveal the hydrogel rings which were then released into solution; the PBS dissolved the sacrificial F127 (Figure 3.1Aii). Collagen laden with primary human umbilical artery smooth muscle cells (HUASMCs) was used to form cell-laden hydrogel rings. A live/dead stain was performed with calcein AM and ethidium homodimer-1, showing the cells maintained excellent viability (Figure 3.1Bi). Further, arrays of hydrogel rings can efficiently be made with this method (Figure 3.1Bii).

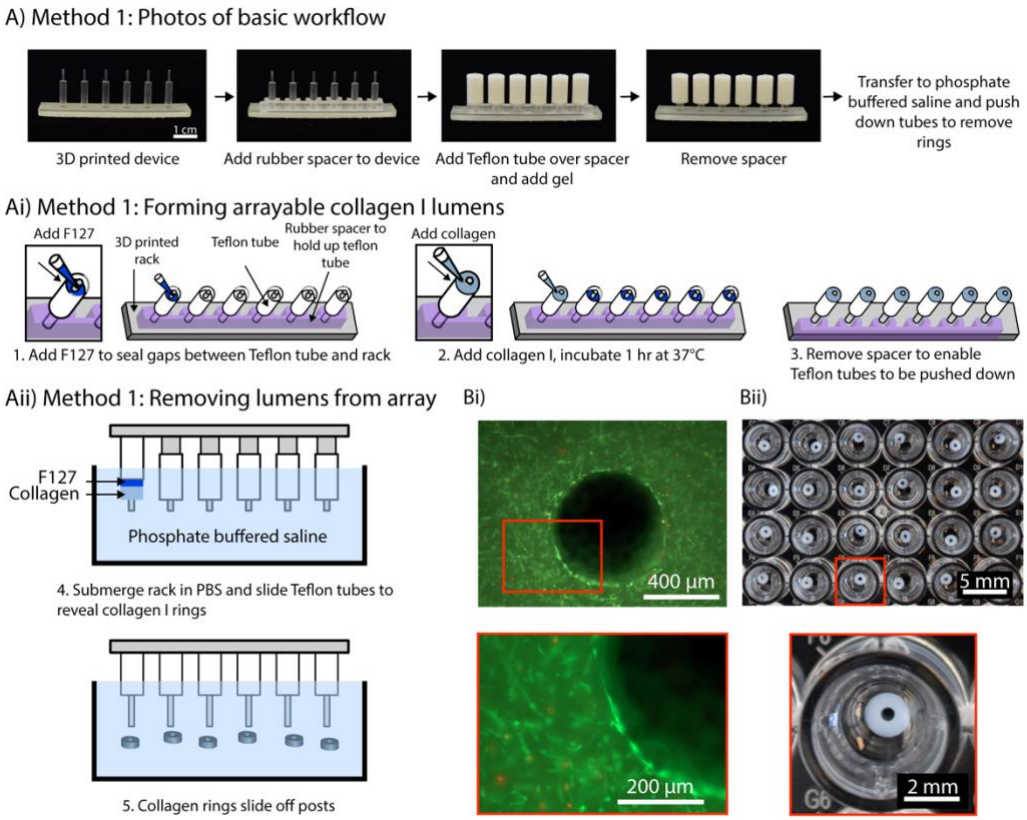

Figure 3.1. An arrayable method for fabricating cell-embedded free-standing collagen I lumens. (Ai) Photographs of device setup and basic workflow for Method 1. (Aii) A rubber spacer was added to the 3D printed device to hold up the Teflon tubes on each post. F127 hydrogel seals small gaps so the collagen I does not leak through. (Aiii) The rack was submerged in phosphate buffered saline, and the tubes were pushed down to remove the collagen rings and dissolve F127. (Bi) Fluorescence image of primary human umbilical artery smooth muscle cells embedded in a collagen I ring. Cells are stained with calcein AM (live, green) and ethidium-homodimer I (dead, red). (Bii) Image of an array of 3 mm OD and 1 mm ID hydrogel rings in a 96-well plate.

We evaluated the reproducibility of this method in two separate experiments with two devices of the same design (12 total collagen rings per experiment) in each experiment. While the rings can fit in a 96-well plate as shown in Figure 3.1B, the light from the imaging set up used to measure the rings reflects off the bottom of the concave meniscus, causing a glare over the collagen ring and impeding proper imaging. In a larger well plate, such as the 24 well plate, a glare was still present when imaging; however due to the larger diameter of the well relative to the collagen ring,

the glare does not cover the ring (Figure 3.2A). This is important because when measuring the ring with ImageJ, the glare and white color of the collagen ring appear the same color which prevents the imaging software from differentiating the two areas.

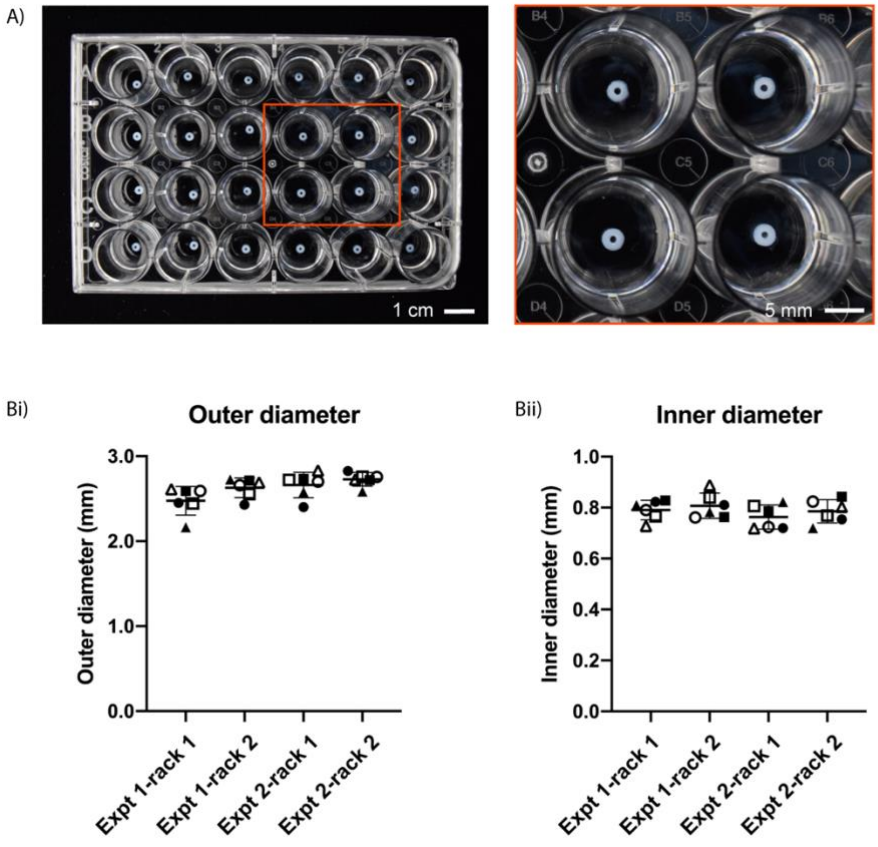

Figure 3.2. Reproducibility of collagen I rings designed with an outer diameter of 3.0 mm and inner diameter of 1.0 mm. (A) Collagen rings of equal size in a 24-well plate. (Bi) The average outer diameter from each device was 2.48±0.17 mm, 2.63±0.12 mm, 2.66±0.15 mm, 2.73±0.08 mm and (Bii) their respective inner diameters were 0.79±0.04 mm, 0.81±0.05 mm, 0.76±0.05 mm, and 0.79±0.05 mm. Each symbol pairs the OD measurements to ID measurements across Bi and Bii. Results are plotted from two independent experiments, each with two racks (one rack is an array of 6 lumens). Error bars are mean ± SD. Full set of data available in Table S2.

The designed dimensions for the collagen rings were 3 mm outer diameter and 1 mm inner diameter. Overall, the actual inner diameter, outer diameter, and wall thickness were smaller than designed (Figure 3.2Bi and 3.2Bii). The average outer diameter for each device ranged from 2.48

to 2.73 mm, a difference of 250 μm and the average inner diameter ranged from 0.76 to 0.81 mm, a difference of 40 μm. The difference can be attributed to the measurement technique (described in the Methods section). Additionally, standard deviations can be attributed to the measurement technique and inherent differences that occur in 3D printed devices. However, ultimately it is not critical to minimize the standard deviation across hydrogel rings because when an assay is performed with the rings the measurement made is the percent change in outer and inner diameter or area over time.

The addition of endothelial cells to line the lumen allows our method to further model the structure of a human blood vessel. Method 1 of creating collagen rings was adapted to make the post removable, enabling an endothelial cell suspension to be added to the lumen after gelation of the hydrogel ring (Figure 3.3). The post was removed and an endothelial cell suspension was pipetted into the lumen, after which the device was incubated for 1 hour. During this incubation period, the device was rotated 180 degrees every 5 minutes for the first 20 minutes and then every 10 minutes for an additional 40 minutes to ensure distribution of cells on all sides of the lumen. The spacer was removed and the Teflon tube was pushed down to reveal the ring with endothelial cells seeded in the lumen. The cells were then incubated in a well plate with cell culture media for 24 hours after which a live/dead stain was performed. Endothelial cells were viable at 24 hours and were evenly distributed within the lumen (Figure 3.3B). Imaging the hydrogel ring due to its free-standing nature can be challenging as it is suspended in liquid media. To increase the usability of this method, future work includes adding a holder to stabilize the ring without restricting its movement in three dimensions.

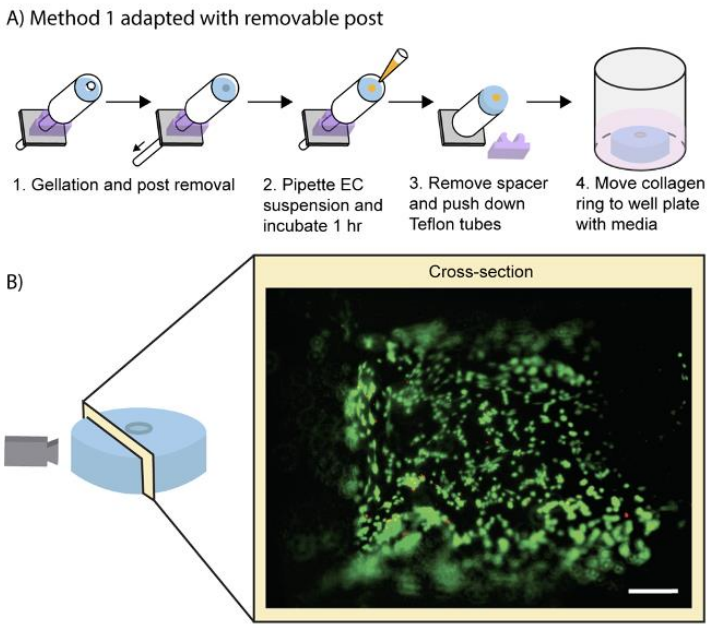

Figure 3.3. Addition of endothelial cells to the lumen of collagen I rings. (A) Workflow for adding the endothelial cell suspension to the gelled collagen rings after adapting Method 1. (B) Image of the lumen was taken after 24 hours of cell seeding to show the viability of the endothelial cells. Cells are stained with calcein AM (live, green) and ethidium-homodimer I (dead, red). Scale bar is 100 µm.

While Method 1 (Figure 3.1) works well for arrayed generation of hydrogel rings, we also sought to develop a method to make individual hydrogel rings with a simpler setup, avoiding the need to use F127 and multiple pieces (spacer, Teflon tubes, etc.). Method 2 uses a commercially available syringe that has been adapted to form collagen rings by cutting off the tip of the syringe and inserting a 3D printed core. Collagen laden with smooth muscle cells was then pipetted into the syringe and incubated to allow the collagen to gel. The 3D printed core was then pushed upwards (Figure 3.4A), revealing the collagen ring, and the ring was transferred to a well plate with cell culture media for storage. Following 5 days in culture, cell-laden hydrogel rings were submerged in a buffer (Tyrode's Solution) and treated with either a control (additional Tyrode's Solution) or a vasodilator (fasudil). The collagen rings were recorded for 20 minutes using a stereoscope to monitor any change in geometry and size. This imaging setup is cost effective (<$500 USD) and

does not require specialized training to record the collagen rings. Images obtained from these recordings were analyzed using ImageJ, a free imaging processing software, to determine the change in percent area of the rings over time (Figure 3.4). A significant difference in ring area was observed when hydrogel rings were treated with a control (buffer) compared to the vasodilator (fasudil). We note that as the cells interact with the hydrogel, the mechanical stress experienced by the cells offers cues for cellular behavior and thus may affect the overall size change. [24, 25]

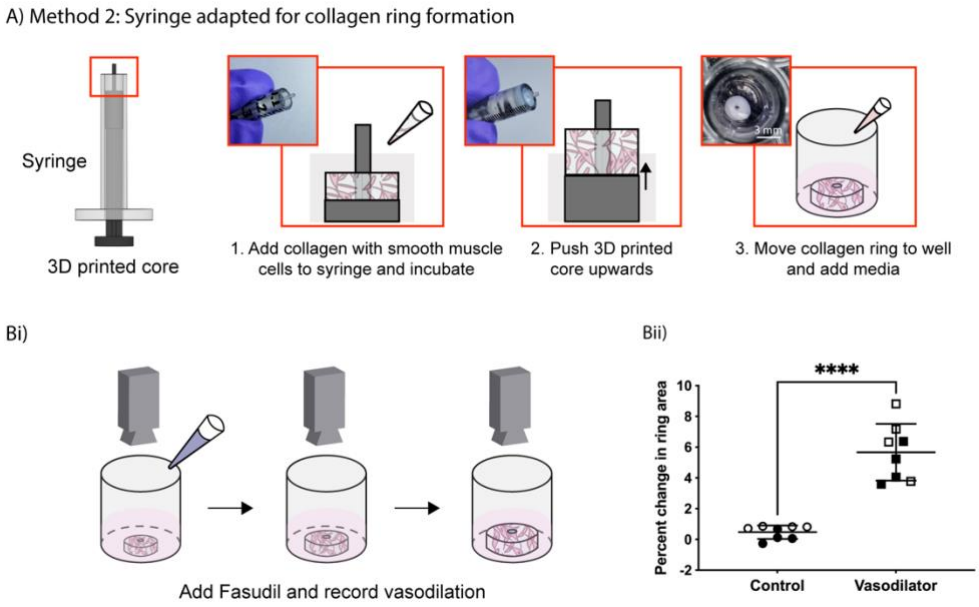

Figure 3.4. Percent change in ring area when human umbilical artery smooth muscle cells seeded in hydrogel rings were treated with a vasodilator (fasudil). (A) Method 2 workflow using a commercially available syringe with a 3D printed insertable core that has been adapted to make cell laden collagen rings. (Bi) The hydrogel rings were recorded for 20 minutes after addition of fasudil, and their percent change in area was calculated using ImageJ. (Bii) Percent change in ring area data for hydrogel rings treated with buffer (control) or vasodilator (fasudil). Data points are from 8 rings across 2 independent experiments; error bars are mean ± SD. A two-sample unpaired t-test (two-tailed) was used. ****$p<0.0001$.

3.1.3 *Methods*

3.1.3.1 Fabrication of device to mold hydrogel rings

Method 1 (Figures 3.1-3): Molds were designed using Solidworks (Dassault Systems, Waltham, MA). Hydrogel ring molds were fabricated using a Form 2 SLA 3D printer (Formlabs, Somerville, MA) using Clear V4 resin (Formlabs) with a Z resolution of 0.05 mm. After printing, molds were cleaned in a FormWash with isopropyl alcohol (IPA) for 10 min, followed by a second wash with fresh IPA for 10 min. Molds were then dried using compressed air and cured under UV (FormCure, Formlabs) for 30 min at 60°C. A 3.5 mm thick polydimethylsiloxane (PDMS) spacer was made by milling a polystyrene mold (Datron Neo) and pouring PDMS (Sylgard™ 184, Dow) in a 1:8 ratio. The PDMS was left to cure at room temperature for 48 h. Prior to use for cell culture, molds were sprayed with 70% ethanol, air dried in a biosafety cabinet, and irradiated with UV light for 15 minutes.

Method 2 (Figure 3.4): Cores were prepared using the same printing and sterilization protocols as Method 1. After posts were UV sterilized in the biosafety cabinet for 20 min, posts were soaked in 1% bovine serum albumin (BSA) for 40 minutes to prevent the collagen from sticking to the post, enabling easier removal of the hydrogel ring, and left to air dry before use. 1 mL syringes (COVIDIEN™) were trimmed at the 0.8 mL mark and the core was replaced with the 3D-printed posts.

3.1.3.2 Cell culture of human umbilical artery smooth muscle cells (HUASMCs) and human umbilical vein endothelial cells (HUVECs)

Human umbilical artery smooth muscle cells (HUASMCs; Cell Applications, Inc) were cultured in human smooth muscle cell growth medium (SmGM; Cell Applications, Inc) supplemented with

penicillin (100 units mL^{-1}) and streptomycin (100 µg mL^{-1}). Human umbilical vein endothelial cells (HUVECs; Lonza) were cultured in endothelial cell growth medium (EGM-2; Lonza) supplemented with penicillin (100 units mL^{-1}) and streptomycin (100 µg mL^{-1}). Culture flasks were maintained at 37 °C with 5% CO_2. HUASMCs between passages 4 and 8 were used; HUVECs between passages 5 and 11 were used.

3.1.3.3 Preparation of collagen I solution

HEPES buffer was prepared as 500 mM in 10X PBS and adjusted to a pH of 7.4 using NaOH pellets. The HEPES buffer was then thoroughly mixed with high concentration collagen I (8 – 10 mg mL^{-1}; Corning) in a 1:9 ratio of HEPES to collagen.

3.1.3.4 Encapsulation of HUASMCs in collagen I hydrogel

HUASMCs were trypsinized and resuspended at a concentration of 5 x 10^6 cells mL^{-1} in growth medium (SmGM). The cell suspension was then added to the neutralized collagen solution for a final concentration of 1 x 10^6 cells mL^{-1} and 6 mg mL^{-1} collagen I.

3.1.3.5 Hydrogel ring fabrication

Method 1 (Figures 3.1-3)

Teflon tubing (McMaster Carr) with an inner diameter of 3.175 mm and an outer diameter of 6.35 mm was cut to 1 cm in length, sonicated in with 70% ethanol for 30 min, air dried, and then transferred onto the 3D printed molds with PDMS spacers. A 20% solution of Pluronic® F127 (P2443–1KG; referred to as F127) (Sigma Aldrich) was pipetted into the mold for the rings and then removed, leaving a thin layer of F127 and filling any gaps between the 3D printed device and the Teflon tubing. The devices were placed in a box with Kimwipes saturated in 1X PBS to prevent evaporation of any hydrogel. The box was placed in a 37 °C incubator for 5 min to fully set the F127. A tube of collagen was warmed up to room temperature to prevent it from dissolving the

F127. The collagen was then pipetted into the molds, the molds placed back in the box with PBS, and incubated for 1 h. To remove the collagen rings the PDMS spacer was removed and the device was submerged in PBS. The Teflon tube was pushed down and the collagen rings were gently removed from the 3D printed post using tweezers or by gently shaking the device. They were then transferred to a 24 well plate with 500 µL of PBS in each well.

Method 2 (Figure 3.4)

For Method 2 the trimmed syringes and BSA soaked 3D printed cores were combined to form the mold. The cell-laden collagen solution was then carefully pipetted into the mold to avoid bubbles; depending on the tubing size, roughly 20 – 30 µL of cell-laden collagen solution was used per ring. After addition of hydrogel mixture, the molds were placed in a BioAssay Dish that was lined with Kimwipes soaked in 1X PBS. The BioAssay Dish containing molds was then transferred to an incubator to allow the collagen to gel at 37 °C. For the first 10 min, the BioAssay Dish was carefully flipped 180° every 2 min to ensure distribution of cells throughout the collagen.

After 1.5 h of incubation, the BioAssay Dish containing hydrogel ring molds was removed from the incubator and brought into a biosafety cabinet. The Teflon tubing was lowered and the hydrogel rings were transferred to individual wells in a 96-well plate. 100 µL of cell culture media was added to each well, and the surrounding wells were filled with 100 µL of 1X PBS to prevent evaporation of media. The hydrogel rings were then incubated at 37 °C with 5% CO_2 until experimentation, with growth media replaced every 24 h.

3.1.3.6 Measurement of hydrogel rings

Images were obtained using an Amscope MU1403B High Speed Microscope Camera mounted on an Amscope SM-3TZ-80S stereoscope (Amscope, Irvine, CA) and processed in FIJI (ImageJ). All

images were thresholded between 40 and 255 prior to obtaining measurements. The outer diameter was measured manually by drawing a line across the image at 0, 45, 90, and 135 degrees and averaging those values; the same procedure was used for the inner diameter.

3.1.3.7 Addition of endothelial cells to hydrogel rings

Using Method I, a 3D printed mold was generated with a hole rather than a post. Teflon tubing (McMaster Carr) was run through each mold to act as a retractable post. Collagen I was added to the mold carefully to avoid bubbles and incubated for 1 h, as outlined above. After 1 h of incubation, the BioAssay Dish containing hydrogel ring molds was removed from the incubator and brought into a biosafety cabinet. The retractable Teflon tubing was then drawn down to reveal a lumen while the hydrogel rings remained in the mold. Approximately 5 µL solution of HUVECs (1×10^6 cells mL^{-1}) was carefully pipetted into the lumen for each ring. The devices were rotated 180 degrees every 5 min for the first 20 min and then 180 degrees every 10 min for the following 40 min to ensure even distribution of HUVECs within the lumen. After 1 h of incubation and rotation, hydrogel rings were removed in a solution of PBS and transferred to a well plate as described above. Each ring was incubated in 60 µL of EGM-2 media for 24 h. At the 24 hour mark rings were washed with PBS and stained with calcein AM (C3100MP, Fisher Scientific) and ethidium-homodimer 1 (E1169, Fisher Scientific) for 30 min at 37 °C, rinsed with PBS, and imaged using a fluorescence microscope (Zeiss Axiovert 200 and an Axiocam 503 mono camera; Carl Zeiss AG, Oberkochen, Germany).

3.1.3.8 Dilation experiments

After 5 days in culture, cell-laden hydrogel rings were used for vasodilation experiments. Two hydrogel rings were transferred to individual wells of a new 96-well plate, and submerged in 60 µL Tyrode's Solution (T2397, Sigma-Aldrich). After 5 min of equilibration the solution was

removed and replaced with fresh Tyrode's Solution. 6 μL of either additional Tyrode's Solution (control) or fasudil (vasodilator) (HA-1077 dihydrochloride, Sigma-Aldrich) was then added. The well plate was then placed under a stereoscope and recorded for 20 min after which hydrogel rings were transferred to a new well plate containing cell media for staining and imaging. This process was repeated with additional hydrogel rings until the desired number of replicates had been tested.

3.1.3.9 Imaging of vasodilation experiments and processing

Top-view images of hydrogel rings were recorded using an Amscope MU1403B High Speed Microscope Camera mounted on an Amscope SM-3TZ-80S stereoscope. Stills were obtained from video recordings for every 60 s (i.e., 21 stills were obtained for a 20 min recording). These images were then processed using FIJI (ImageJ) to calculate the total hydrogel area.

3.1.4 *Conclusion*

We demonstrate that we have created a simple method for forming freestanding cell-laden hydrogel rings that can be used in a quantifiable assay for measuring dynamic change after treatment with a known vasodilator. Our goal was to create a method that does not rely on animal models or rigid devices to stabilize the lumen. Our method takes the unique approach to being freestanding which allows unrestricted movement in all three dimensions in response to vasoactive compounds. This method enables researchers to study the response of a controlled human cell-laden hydrogel ring to different inflammatory drugs or molecules, as well as study the cellular communication that is important to understanding the pathways that are activated during inflammation. So far, we have only tested the model with fasudil; additional vasodilators and vasoconstrictors would need to be tested to further validate our method for use in vasodilator and vasoconstrictor studies. Additionally, alignment of the smooth muscle cells was not achieved in this current work. This will be a focus of future work to ensure smooth muscle cells are able to

constrict and dilate while in the alignment observed in blood vessels. In future work we will also work to achieve lumen size and wall thickness relevant to smaller vessels in the human body. We anticipate this can be addressed using higher resolution fabrication methods. Additionally, we will integrate these freestanding lumens with other co- and multiculture platforms to incorporate fibroblasts, smooth muscle cells, endothelial cells, and other stromal cells important for modeling disease-specific vasodilation, as well as cell types in circulating blood including leukocytes that may interact with endothelial cells and be recruited to neighboring tissue. We envision that our model will be important for studying a range of diseases such as asthma, cancer, autoimmune disease, and other diseases that have periods of induced inflammation, vasodilation, or constriction.

3.1.5 *References*

1. Horvath, G.; Wanner, A., Inhaled corticosteroids: effects on the airway vasculature in bronchial asthma. *European Respiratory Journal* **2006,** *27* (1), 172-87.
2. Duval, K.; Grover, H.; Han, L.-H.; Mou, Y.; Pegoraro, A. F.; Fredberg, J.; Chen, Z., Modeling Physiological Events in 2D vs. 3D Cell Culture. *Physiology* **2017,** *32* (4), 266-277.
3. Edmondson, R.; Broglie, J. J.; Adcock, A. F.; Yang, L., Three-dimensional cell culture systems and their applications in drug discovery and cell-based biosensors. *ASSAY and Drug Development Technologies* **2014,** *12* (4), 207-18.
4. Tibbitt, M. W.; Anseth, K. S., Hydrogels as extracellular matrix mimics for 3D cell culture. *Biotechnology and Bioengineering* **2009,** *103* (4), 655-63.
5. Bischel, L. L.; Sung, K. E.; Jiménez-Torres, J. A.; Mader, B.; Keely, P. J.; Beebe, D. J., The importance of being a lumen. *The FASEB Journal* **2014,** *28* (11), 4583-90.
6. Pampaloni, F.; Reynaud, E. G.; Stelzer, E. H., The third dimension bridges the gap between cell culture and live tissue. *Nature Reviews Molecular Cell Biology* **2007,** *8* (10), 839-45.
7. Jia, W.; Gungor-Ozkerim, P. S.; Zhang, Y. S.; Yue, K.; Zhu, K.; Liu, W.; Pi, Q.; Byambaa, B.; Dokmeci, M. R.; Shin, S. R.; Khademhosseini, A., Direct 3D bioprinting of perfusable vascular constructs using a blend bioink. *Biomaterials* **2016,** *106*, 58-68.
8. Marceau, F.; deBlois, D.; Petitclerc, E.; Levesque, L.; Drapeau, G.; Audet, R.; Godin, D.; Larrivée, J. F.; Houle, S.; Sabourin, T.; Fortin, J. P.; Morissette, G.; Gera, L.; Bawolak, M. T.; Koumbadinga, G. A.; Bouthillier, J., Vascular smooth muscle contractility assays for inflammatory and immunological mediators. *International Immunopharmacology* **2010,** *10* (11), 1344-53.

9. Pi, Q.; Maharjan, S.; Yan, X.; Liu, X.; Singh, B.; van Genderen, A. M.; Robledo-Padilla, F.; Parra-Saldivar, R.; Hu, N.; Jia, W.; Xu, C.; Kang, J.; Hassan, S.; Cheng, H.; Hou, X.; Khademhosseini, A.; Zhang, Y. S., Digitally Tunable Microfluidic Bioprinting of Multilayered Cannular Tissues. *Advanced Materials* **2018,** *30* (43), 1706913.
10. Zhang, Y.; Yu, Y.; Akkouch, A.; Dababneh, A.; Dolati, F.; Ozbolat, I. T., In Vitro Study of Directly Bioprinted Perfusable Vasculature Conduits. *Biomaterials Science* **2015,** *3* (1), 134-43.
11. Tseng, H.; Gage, J. A.; Haisler, W. L.; Neeley, S. K.; Shen, T.; Hebel, C.; Barthlow, H. G.; Wagoner, M.; Souza, G. R., A high-throughput in vitro ring assay for vasoactivity using magnetic 3D bioprinting. *Scientific Reports* **2016,** *6* (1), 30640.
12. Badesch, M. D. D. B., Clinical Trials in Pulmonary Hypertension *Annual Review of Medicine* **1997,** *48* (1), 399-408.
13. Impellizzeri, D.; Bruschetta, G.; Esposito, E.; Cuzzocrea, S., Emerging drugs for acute lung injury. *Expert Opinion on Emerging Drugs* **2015,** *20* (1), 75-89.
14. Leuchte, H. H.; Baezner, C.; Baumgartner, R. A.; Bevec, D.; Bacher, G.; Neurohr, C.; Behr, J., Inhalation of vasoactive intestinal peptide in pulmonary hypertension. *European Respiratory Journal* **2008,** *32* (5), 1289.
15. Alford, P. W.; Nesmith, A. P.; Seywerd, J. N.; Grosberg, A.; Parker, K. K., Vascular smooth muscle contractility depends on cell shape. *Integr Biol (Camb)* **2011,** *3* (11), 1063-1070.
16. Fernandez, C. E.; Yen, R. W.; Perez, S. M.; Bedell, H. W.; Povsic, T. J.; Reichert, W. M.; Truskey, G. A., Human Vascular Microphysiological System for in vitro Drug Screening. *Scientific Reports* **2016,** *6* (1), 21579.
17. Hald, E. S.; Steucke, K. E.; Reeves, J. A.; Win, Z.; Alford, P. W., Long-term vascular contractility assay using genipin-modified muscular thin films. *Biofabrication* **2014,** *6* (4), 045005.
18. Jung, Y.; Ji, H.; Chen, Z.; Fai Chan, H.; Atchison, L.; Klitzman, B.; Truskey, G.; Leong, K. W., Scaffold-free, Human Mesenchymal Stem Cell-Based Tissue Engineered Blood Vessels. *Scientific Reports* **2015,** *5* (1), 15116.
19. Steucke, K. E.; Tracy, P. V.; Hald, E. S.; Hall, J. L.; Alford, P. W., Vascular smooth muscle cell functional contractility depends on extracellular mechanical properties. *Journal of Biomechanics* **2015,** *48* (12), 3044-51.
20. Manning, K. L.; Feder, J.; Kanellias, M.; Murphy, J.; Morgan, J. R., Toward Automated Additive Manufacturing of Living Bio-Tubes Using Ring-Shaped Building Units. *SLAS TECHNOLOGY: Translating Life Sciences Innovation* **2020,** *25* (6), 608-620.
21. Strobel, H. A.; Calamari, E. L.; Alphonse, B.; Hookway, T. A.; Rolle, M. W., Fabrication of Custom Agarose Wells for Cell Seeding and Tissue Ring Self-assembly Using 3D-Printed Molds. *J Vis Exp* **2018,** (134), 56618.
22. Lee, U. N.; Su, X.; Guckenberger, D. J.; Dostie, A. M.; Zhang, T.; Berthier, E.; Theberge, A. B., Fundamentals of rapid injection molding for microfluidic cell-based assays. *Lab on a Chip* **2018,** *18* (3), 496-504.
23. Spiers, A.; Padmanabhan, N., A guide to wire myography. *Methods in Molecular Medicine* **2005,** *108*, 91-104.

24. Wei, Q.; Wang, S.; Han, F.; Wang, H.; Zhang, W.; Yu, Q.; Liu, C.; Ding, L.; Wang, J.; Yu, L.; Zhu, C.; Li, B., Cellular modulation by the mechanical cues from biomaterials for tissue engineering. *Biomaterials Translational* **2021,** *2* (4), 323-342.
25. Murtada, S.-I.; Kawamura, Y.; Li, G.; Schwartz, M. A.; Tellides, G.; Humphrey, J. D., Developmental origins of mechanical homeostasis in the aorta. *Developmental Dynamics* **2021,** *250* (5), 629-639.

3.2 3D Printed Coaxial Nozzles for the Extrusion of Hydrogel Tubes Toward Modeling Vascular Endothelium

Reproduced in part from S. C. Millik, A. M. Dostie, D. G. Karis, P. T. Smith, M. McKenna, N. Chan, C. D. Curtis, E. Nance, A. B. Theberge,[§] A. Nelson,[§] "3D printed coaxial nozzles for the extrusion of hydrogel tubes toward modeling vascular endothelium." Biofabrication, **2019***, 11, 045009.*
[§] Corresponding authors

3.2.1 *Overview*

Lumen are ubiquitous in biological systems such as the vasculature, gastrointestinal tract, lymphatic system, and lungs. Fabrication of perfusable structures using biofunctional materials and compatible manufacturing processes is of great interest in the areas of bioengineering (e.g. for *in vitro* assays) and regenerative medicine.[1-4] While there are many different methods for fabricating tubular structures, extrusion based processes provide a facile method to produce complex geometries.[2,4,5] As 3D printers become more common in academic laboratories or shared spaces, a protocol utilizing modifiable 3D printed materials could make extrusion of hydrogel tubes more accessible across laboratories.

Recently, Pi et. al.[2] have demonstrated coaxial extrusion-based fabrication of circumferentially layered tissue-engineered tubular constructs using materials based on methacrylated gelatin, alginate, and acrylated multi-arm poly(ethylene glycol). The authors produced these constructs using urothelial cells, vascular endothelial cells, and smooth muscle cells. These tissue-engineered

constructs represent an important step toward creating engineered replacements for tubular biological structures. However, this platform involves handmade nozzles, which may restrict the platform's accessibility and customizability.

In this work, a practical and versatile 3D printing-enabled platform for the extrusion-based fabrication of tubular hydrogel constructs and multi-material coaxial filaments was designed.[6] This method utilized a 3D printed coaxial nozzle that enable the coextrusion of two hydrogels simultaneously: the sacrificial core hydrogel was comprised of Pluronic F127, while the outer shell hydrogel was cross-linkable F127-bisurethane methacrylate (F127-BUM). Coextrusion of these two hydrogels followed by treatment with UV light to cross-link the F127-BUM generated a hydrogel tube once the sacrificial F127 core was dissolved in solution. A variety of experiments were performed on the properties of the hydrogel tubes, including reproducibility, alternative dimensions, and different shaped lumen. These experiments were primarily the work of Millik, and as such have been excluded from this report. Biological experiments involving the addition of collagen to the F127-BUM tubes resulted in successful addition of endothelial cells to the luminal surface of hydrogel tubes; those results are reported herein.

3.2.2 *Results – Seeding Endothelial Cells on F127-BUM Hydrogels*

Primary human umbilical vein endothelial cells (HUVECs) were seeded onto the F127-BUM polymer in order to determine the compatibility of the F127-BUM polymer as a substrate for endothelial cell adhesion and growth. Initial cell seeding experiments were performed on F127-BUM hydrogel discs, ~5 mm in diameter, that had been cured and washed several times with both PBS and endothelial cell growth medium. HUVECs were seeded at high seeding densities (~1 x 105 cells per disc) to ensure a confluent surface. We used calcein AM, which stains the cytoplasm of live cells, to enable visualization of cell morphology (Figure 3.5A). When endothelial cells were

seeded directly onto the flat surface of F127-BUM polymer discs and cultured in a 96-well plate, cells retained a rounded morphology and did not adhere to the material (Figure 3.5Ai).

In order to promote cell adhesion to F127-BUM polymer, collagen I was used as an additive prior to extrusion of hydrogel tubes. While the incorporation of collagen I with F127-BUM improved the adhesion of HUVECs to the polymer, further coating with collagen I post-fabrication of discs or tubes allowed for a larger incorporation of collagen I and thus greater number of attachment sites for cells. HUVECs seeded on F127-BUM hydrogel discs that were fabricated with collagen I and coated post-fabrication demonstrated adhesion to the discs, visualized by a more spread out cell morphology (Figure 3.5Aii). Beyond adhesion of the endothelial cells to the hydrogel, viability was assessed across multiple days on hydrogel discs; a live/dead assay performed at 72 h indicated satisfactory viability (Figure 3.5Aiii).

Following successful adhesion and culture of HUVECs for multiple days on hydrogel discs, hydrogel tubes comprised of F127-BUM with collagen I additive and coated with additional collagen I were extruded for further experiments. HUVECs were added to the luminal surface of hydrogel tubes and stained with endothelial cell junction marker CD31 (also referred to as platelet endothelial cell adhesion molecule (PECAM-1)) to assess morphology after 72 h in culture. Figure 3.5B shows the expression of CD31 between HUVECs, demonstrating appropriate endothelial cell morphology. Re-constructions of images obtained using confocal microscopy show the coating of endothelial cells on the luminal surface, enabling visualization of the hydrogel tube (Figure 3.5C).

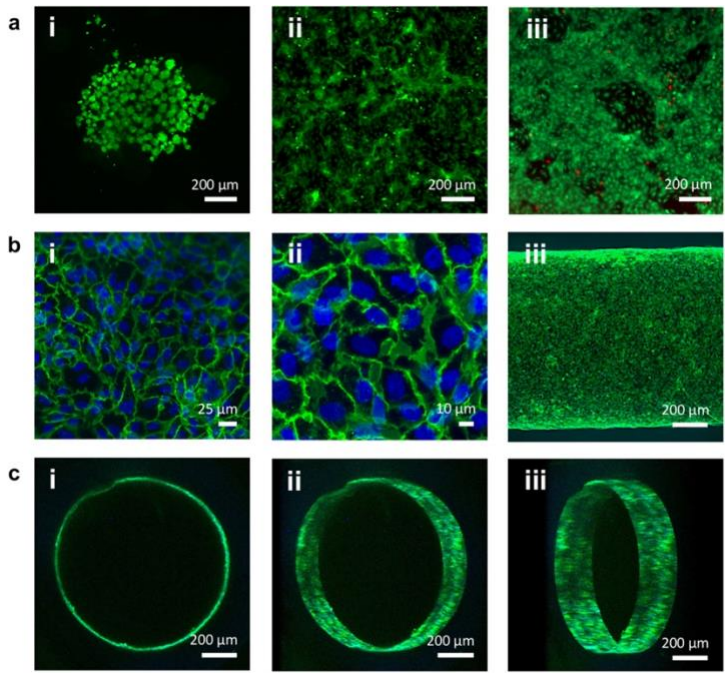

Figure 3.5. Characterization of human umbilical vein endothelial cell (HUVEC) behavior when seeded on polymer material and visualization of cell-seeded hydrogel tubes. (Ai) HUVECs seeded on discs made of cross-linked F127-BUM without collagen additive imaged after 24 h in culture. Cells were incubated with calcein AM (green) to visualize cell morphology, which remained rounded and aggregated, indicating lack of adhesion. (Aii) HUVECs seeded on discs made of cross-linked F127-BUM with collagen additive imaged at 24 h, and (Aiii) at 72 h show an adhered morphology and good viability. Cells were incubated with calcein AM (green) and ethidium homodimer-1 (red) to visualize cell morphology and viability. (B) Morphology of endothelial cells lining the lumen of hydrogel tubes at 72 h. Cells were stained for tight junction marker CD31 (green) and nuclear stain DAPI (blue). (C) Confocal z-stack reconstructions showing good cell coverage of the luminal surface of hydrogel tubes. Images in (A) are representative of three replicates; images in (B) and (C) are representative of six replicates.

3.2.3 *Methods*

Note: Detailed methods for the preparation of F127-BUM, 3D printing of coaxial nozzles, and extrusion through coaxial nozzles can be found in Millik 2019. Those protocols were primarily performed by Millik, and as such have been excluded from this exam report.

3.2.3.1 Cell Culture of HUVECs

Primary human umbilical vein endothelial cells (HUVECs; Lonza) were cultured in endothelial cell growth media (EGM-2; Lonza) supplemented with penicillin (100 units mL^{-1}) and streptomycin (100 µg mL^{-1}). Culture flasks were maintained at 37°C with 5% CO_2. HUVECs were used between passage numbers 4-8 for all experiments. For all cell culture experiments, HUVECs were trypsinized and resuspended at a concentration of 1.0 x 10^6 cells mL^{-1} in EGM-2.

3.2.3.2 Preparation of hydrogel discs and tubes

Prior to cell culture, hydrogel discs and tubes were prepared with collagen I to promote adhesion of cells. Briefly, collagen I was mixed with F127-BUM and incubated on ice until the solution was homogeneous. The collagen was added such that its final concentration in the hydrogel mixture was 2% by weight. The hydrogel mixture was then either cured in a sheet (in the case of the hydrogel discs), or extruded through coaxial nozzles and cured to generate a hydrogel tube. Following curing, hydrogel tubes and discs were dehydrated at 37°C, and re-hydrated in a collagen solution (6 mg mL^{-1}). The re-hydrated tubes and discs were then briefly exposed to ammonia vapor to promote cross-linking of the collagen, and thus retention of collagen within the hydrogel tubes or discs. This procedure was repeated once more, including dehydration, rehydration, and cross-linking. Finally, hydrogel tubes and discs were dehydrated and rehydrated in EGM-2 and stored until used for experiments.

3.2.3.3 Cell seeding and culture on hydrogel discs

Hydrogel discs 5 mm in diameter were placed in individual wells in a 96-well plate, covering the majority of the well bottom (6 mm in diameter). A 100 µL cell suspension was pipetted directly onto the hydrogel discs, and an additional 50 µL of media was added to the well. To prevent

evaporation, surrounding wells were filled with 100µL of 1X PBS. Plates were incubated at 37°C with 5% CO_2, with full media replacement every 24 h until the end of experiment at 72 h.

3.2.3.4 Cell seeding and culture in hydrogel tubes

To facilitate direct addition of endothelial cells to the luminal surface of hydrogel tubes, 1 mL syringes with sterilized blunt-tip needles were utilized; syringes were placed in a 3D printed holder for controlled rotation. Hydrogel tubes were gently transferred onto the needle tip, and the syringe was used to draw EGM-2 into and through the hydrogel tubes. After drawing in media, approximately 100 µL of 1.0 x 10^6 cell mL^{-1} was drawn through the hydrogel tubes such that the lumen were filled with cell suspension. To prevent loss of cell suspension, hydrogel tubes were kept attached to the needles and syringes during initial incubation.

Following addition of cell suspension, syringe/hydrogel tube apparatuses were transferred to a BioAssay Dish lined with Kimwipes soaked in 1X PBS to prevent evaporation. The BioAssay Dish was then incubated at 37°C with 5% CO_2 for 1 h, except for removal every 15 min to manually rotate the syringes/hydrogel tubes 90° to ensure uniform adhesion of endothelial cells on the luminal surface. Following the 1 h incubation, hydrogel tubes were gently removed from the syringes and transferred to individual wells of a 6-well plate; 2 mL of EGM-2 was added to each well. Plates were incubated at 37°C with 5% CO_2, with full media replacement at 48 h.

3.2.3.5 Cell staining and imaging

Cells cultured on hydrogel discs were assessed for adhesion and viability of cells across multiple timepoints. Media was removed from wells and discs were rinsed once with 1X PBS. A solution of calcein AM (0.01 mM) and ethidium homodimer-1 (2 mM) in 1X PBS was then added to each well, and plates were incubated at 37°C with 5% CO_2 for 20 minutes. Following this incubation, discs were immediately imaged using fluorescence microscopy (Zeiss Axiovert 200 with Axiocam

503 mono camera). Images assessed for adhesion by staining with calcein AM were processed in ImageJ and thresholded between 18 and 255 to remove any artifacts from being detected; the thresholded area was determined to measure the coverage of cells.

For immunocytochemistry staining, cell media was removed from wells, replaced with 4% paraformaldehyde, and incubated at room temperature for 20 min. Following fixation, cells were rinsed with 1X PBS three times and treated with permeabilization buffer (20 min), blocking buffer (1 h), and then left overnight at 4°C in a solution of primary antibody (mouse anti-human CD31) in blocking buffer. The following morning cells were washed with washing buffer three times, treated with secondary antibody (Alexa Fluor 488-goat anti-mouse) for 1 h at room temperature. Cells were again washed with washing buffer, incubated with DAPI at room temperature for 5 minutes, and washed with washing buffer; finally, wells were filled with 1X PBS for storage. Stained hydrogel tubes were imaged on a confocal microscope (Nikon AR1 with cMOS camera).

3.2.4 *References*

1. D. B. Kolesky, K. A. Homan, M. A. Skylar-Scott, J. A. Lewis, “Three-dimensional bioprinting of thick vascularized tissues.” *PNAS*, 2016, **113**, 3179
2. Q. Pi et. al. “Digitally tunable microfluidic bioprinting of multilayered cannular tissues.” *Adv. Mater.*, 2018, **30**, 1706913
3. K. H. Song, C. B. Highley, A. Rouff, J. A. Burdick, “Complex 3D-printed microchannels within cell-degradable hydrogels.” *Adv. Funct. Mater.*, 2018, **28**, 1801331
4. Y. Zhang, Y. Yu, A. Akkouch, A. Dababneh, F. Dolati, I. T. Ozbolat, “In vitro study of directly bioprinted perfusable vasculature conduits.” *Biomater. Sci.*, 2015, **3**, 134
5. W. Jia et. al. “Direct 3D bioprinting of perfusable vascular constructs using a blend bioink.” *Biomaterials*, 2016, **106**, 58
6. S. C. Millik, A. M. Dostie, D. G. Karis, P. T. Smith, M. McKenna, N. Chan, C. D. Curtis, E. Nance, A. B. Theberge§, A. Nelson§, “3D printed coaxial nozzles for the extrusion of hydrogel tubes toward modeling vascular endothelium.” *Biofabrication*, 2019. **11**, 045009

Chapter 4. COVID-19 PRE-SYMPTOMATIC STUDY

4.1 INTRODUCTION

The worldwide pandemic of COVID-19 greatly altered the way humans interact with each other, including isolation and working remotely to avoid contracting severe acute respiratory syndrome coronavirus 2 (SARS-CoV-2). Even prior to 2020, researchers were developing devices that could be used for at home care, either for immediate diagnostic use (such as an at home pregnancy test) or for later diagnosis in a doctor's office or laboratory (such as genetic testing). At-home tests for COVID-19 or for genetic testing typically require a nasal or saliva sample. Blood collection has typically required a laboratory or clinical setting due to the complexity involved with venipuncture. Remote blood collection is of particular interest as it allows individuals to collect a sample without needing to schedule an appointment or commute to a different location.

Recently, the Theberge lab designed and optimized an at-home blood collection kit known as *home*RNA.[1] The *home*RNA kits contain a commercially available blood collection device (the Tasso-SST™ device) and a stabilizer tube designed by the Theberge lab. In the pilot study, *home*RNA kits were shipped to participants in several US states.[1] Participants collected a blood sample using the Tasso-SST™, then transferred the blood collected from the Tasso-SST™ to the stabilizer tube designed by the Theberge lab. This secondary tube contained a commercial stabilization solution. After mixing the blood sample with the stabilizing reagent, the sample could then be sent to a research laboratory and analyzed at a later date. The stabilization solution works by stabilizing any RNA present in the sample, preventing degradation of RNA between blood collection and analysis within the lab. At the time of sample collection participants reported feedback including device usability and pain levels; then, participants shipped the sample back to the Theberge lab using the packaging materials that were included with the kit. The pilot

*home*RNA study performed by Haack et al. primarily focused on optimizing the stabilization tube and testing multiple stabilization solutions, ensuring that the blood collected was stable and able to be analyzed for RNA at a later time.

Here, we use the *home*RNA kit in a longitudinal study for individuals who are either (1) exposed to COVID-19, or (2) test positive for COVID-19 but are asymptomatic. It is difficult to obtain a blood sample of an individual prior to an immune response to a viral infection, as the individual may not be aware that they are sick. The recruitment for this study thus focused on individuals as described above; upon exposure to COVID-19, an individual knows they may contract the disease. By participating in our study, the individual is able to provide samples prior to an immune response; the *home*RNA kit facilitates collection of these samples by enabling participants to collect blood samples at home, removing any barrier related to traveling to a clinic for sampling. This study follows eligible participants for 28 days to study the immune response of individuals after exposure and/or before the onset of symptoms, as well as track the immune response over the course of infection. Participants collected both nasal and blood samples and reported any current symptoms they experienced using a secure survey sent to their phone or email. As this study is currently ongoing, this chapter will describe the study design and preliminary data including participant demographics and usability of the nasal and blood collection kits.

4.2 Study Design

This study was approved by the University of Washington Institutional Review Board (IRB) under protocol STUDY00007868.

The purpose of this study is to monitor the immune response of a participant who is either pre-symptomatic or asymptomatic, and follow the immune response as the participant either develops symptoms or remains asymptomatic. Due to the potentially small timeframe that a participant is

pre-symptomatic or asymptomatic, once an individual's eligibility was confirmed and they were enrolled, a study kit was sent to the individual as quickly as possible. For example, if an individual enrolled in the study in the morning, the study team worked to confirm eligibility and shipped out the study kit that same afternoon, using overnight shipping so the participant received the study kit the next morning.

The timeline for this pre-symptomatic study includes sample collection for 10 days over the course of a month, or 28 days (Figure 4.1). For the first seven days the participant collected a blood sample, a nasal sample, and completed a symptom survey each day. After the initial week, participants only collected one blood sample and completed one symptom survey per week on days 14, 21, and 28.

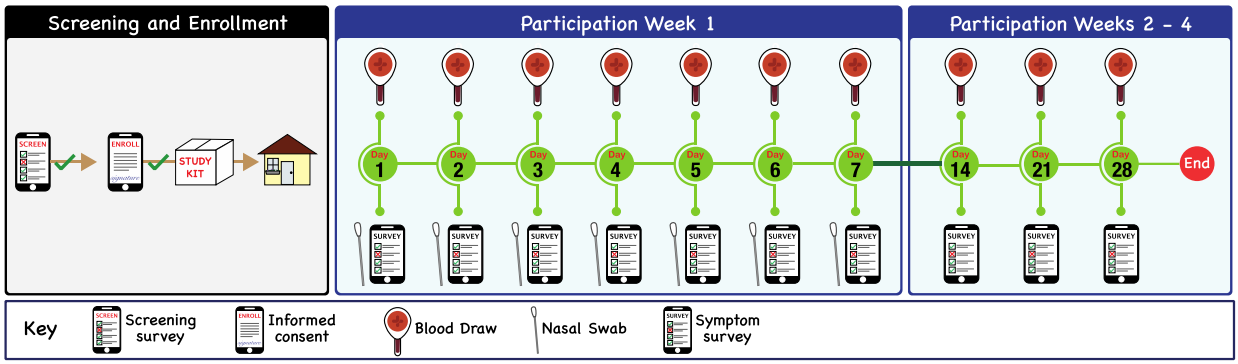

Figure 4.1. Timeline for pre-symptomatic study (Courtesy of Fang Yun Lim)

The first nasal swab collected by participants was sent to Kashi Laboratories, a Clinical Laboratory Improvement Amendments (CLIA) Certified lab that was contracted by the Theberge lab for reverse transcription-polymerase chain reaction (RT-PCR) detection of SARS-CoV-2 viral load. Because participants in this study have either tested positive for COVID-19 or were recently exposed, the Kashi Labs is able to analyze samples for SARS-CoV-2 and report the test results to state authorities across the country. The Kashi Labs also have a licensed physician who can provide a phone consultation for all positive and indeterminate results.

All other nasal swab samples were returned to the study team at UW and frozen until analysis at the end of the study. Samples will then be tested for SARS-CoV-2 viral load as well as the viral load of other respiratory viruses; these results will not be returned to study participants. Aside from the Day 1 nasal swab, all nasal swabs were sent back to the Theberge Lab with the corresponding daily blood sample. Blood samples will also be stored until analysis at the end of the study, at which time RNA will be extracted and analyzed.

4.3 Enrollment of Participants

Passive recruitment was used for enrollment and included digital advertisements as well as word of mouth. Individuals who believed they were eligible for the study completed the initial Eligibility Screen hosted on Research Electronic Data Capture (REDCap), a platform developed by the Institute of Translational Health Sciences for secure human subjects. REDCap allowed for remote recruitment and enrollment.

In order to be eligible for this study, participants must be adults over the age of 18; must not be immunosuppressed; and must not currently reside in a correctional facility. In addition to confirming these requirements, the Eligibility Screen asked about vaccination status, potential exposure to COVID, and any potential symptoms the individual was currently experiencing. If an individual was deemed eligible based on their responses to these questions, they then provided their contact information and were invited to enroll in the study.

If an individual indicated they were interested in enrolling, they were next taken to an Informed Consent Form (ICF). The ICF enabled the individual to fully consent in the study by providing information about the study, collection methods, and compensation. Additionally, study team members were available by phone or email to answer any questions individuals may have had

about the study. As participation in this study required an ICF, incorporation of the ICF within REDCap eliminated the need for phone calls between the study team and potential participants. This prevented a potential lapse in time between the Eligibility Screen and participant enrollment, aiding the study team's goal in obtaining samples while a participant is still pre-symptomatic.

While this study is ongoing, to date the Eligibility Screen has received 1380 Record IDs, indicating up to 1380 individuals accessing the Eligibility Screen and at least partially completing the survey. As seen in Figure 2, the extent of reach through passive recruitment resulted in at least one survey from each of the states in the US as well as in DC (Figure 4.2). Not all 1380 Record IDs provided a Zipcode; as such, the data provided in Figure 2 is from 1216 Eligibility Screen Responses.

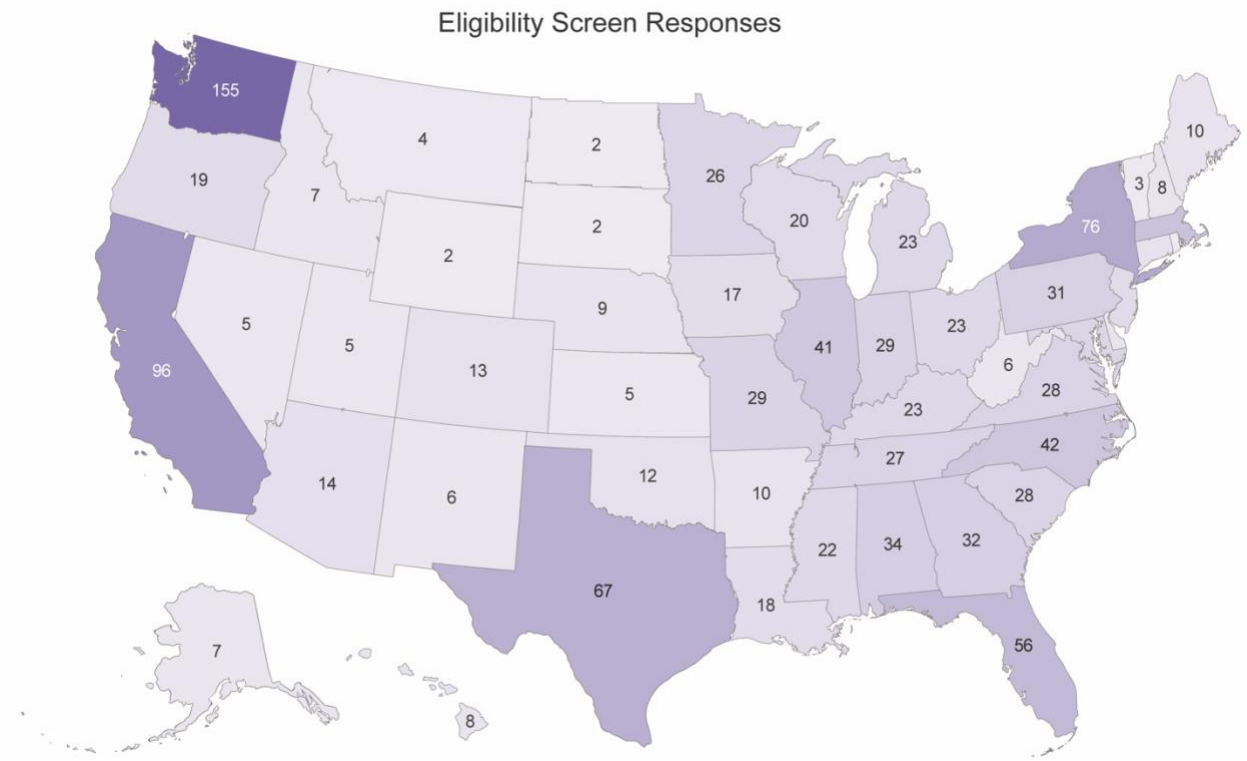

Figure 4.2. U.S. Map of Eligibility Screen Responses. All states (and Washington D.C.) had at least one response to the Eligibility Screen (n = 1216).

Upon *completion* of the ICF, eligible participants then completed the Welcome Survey that requested information including any COVID test results and demographic information such as age, sex, ethnicity, and race (Figure 4.3). Of the 135 eligible individuals who provided their sex assigned at birth, 71% indicated their sex was female. Interestingly, the demographics for race are similar to the most recent US Census Bureau report from 2021 (Figure 4.3D).

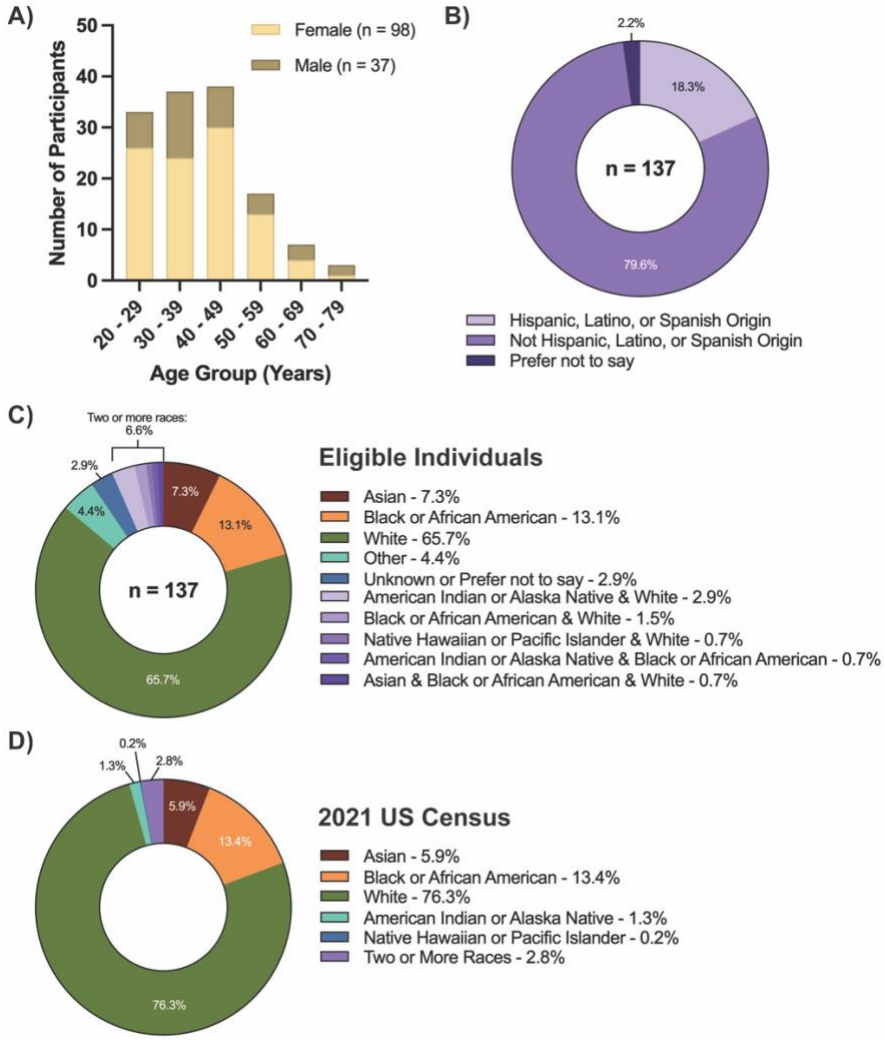

Figure 4.3. Demographic information for eligible individuals. A) Age and sex demographics by age group (n = 135). B) Ethnic demographics (n = 137). C) Race demographics (n = 137). D) Race demographics from the 2021 U.S. Census.

After individuals completed the Welcome Survey, the study team decided whether to enroll the individual as a participant or to exclude them based on pre-determined criteria. In the case of an

exclusion, an individual consented to the study but were not enrolled in the study following secondary screening. The most common cause for exclusion was when the study team was unable to contact the individual; additional reasons include multiple entries with inconsistent information and failure to complete enrollment by not providing the required information. Of 1380 survey responses, 148 surveys were eligible for enrollment – 65 of these were excluded (Figure 4.4).

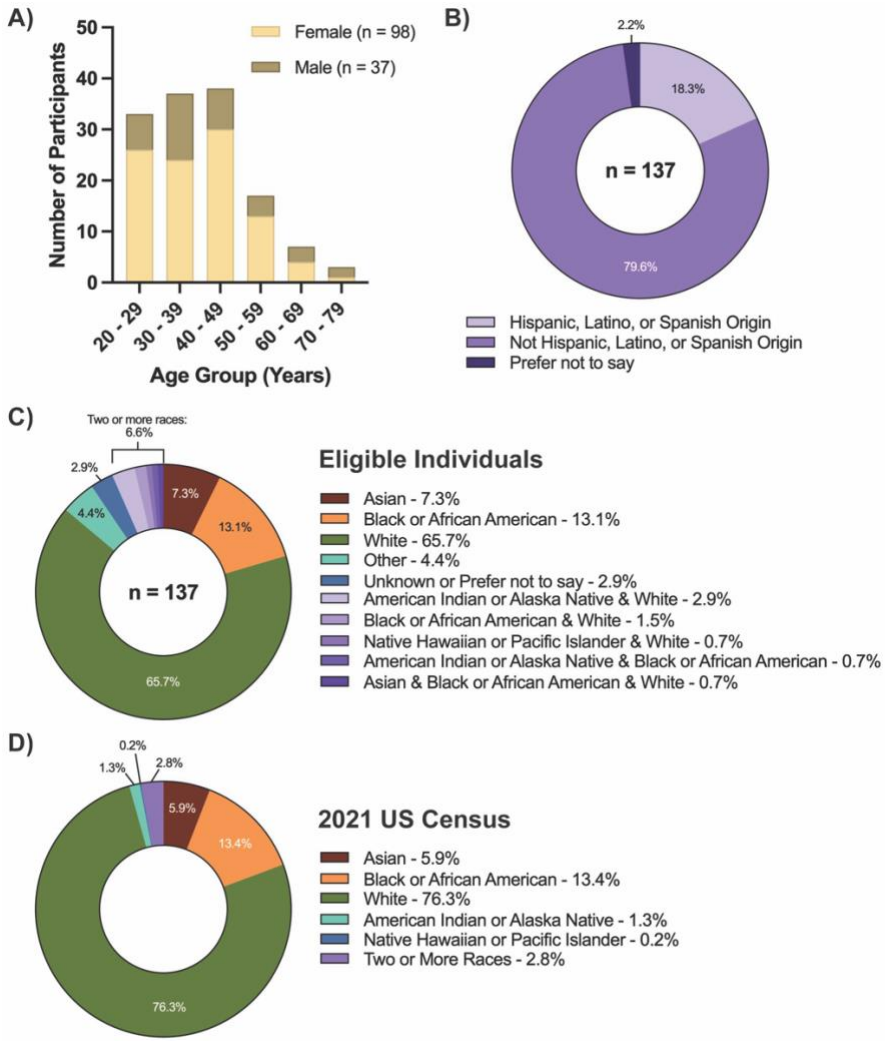

Figure 4.4. Enrollment, withdrawal, and exclusion of eligible participants.

Of the 83 participants who were enrolled, 16 have been withdrawn from the study. A withdrawal occurs when a participant received a study kit but was unable to complete the study; this includes

participants who collected multiple samples as well as those who were unable to collect any sample. Reasons for withdrawal included participants uncomfortable with using the blood collection device, as well as some individuals deciding not to continue with sampling after the first or second day of collection.

At the time of writing 61 participants have completed their participation, including several cases of extended sampling where participants provided additional blood samples. These participants ranged across 26 different states in the US (Figure 4.5), varying from rural to metropolitan areas. The age and sex, ethnicity, and race demographics for the participants who completed the study are shown in Figure 4.6.

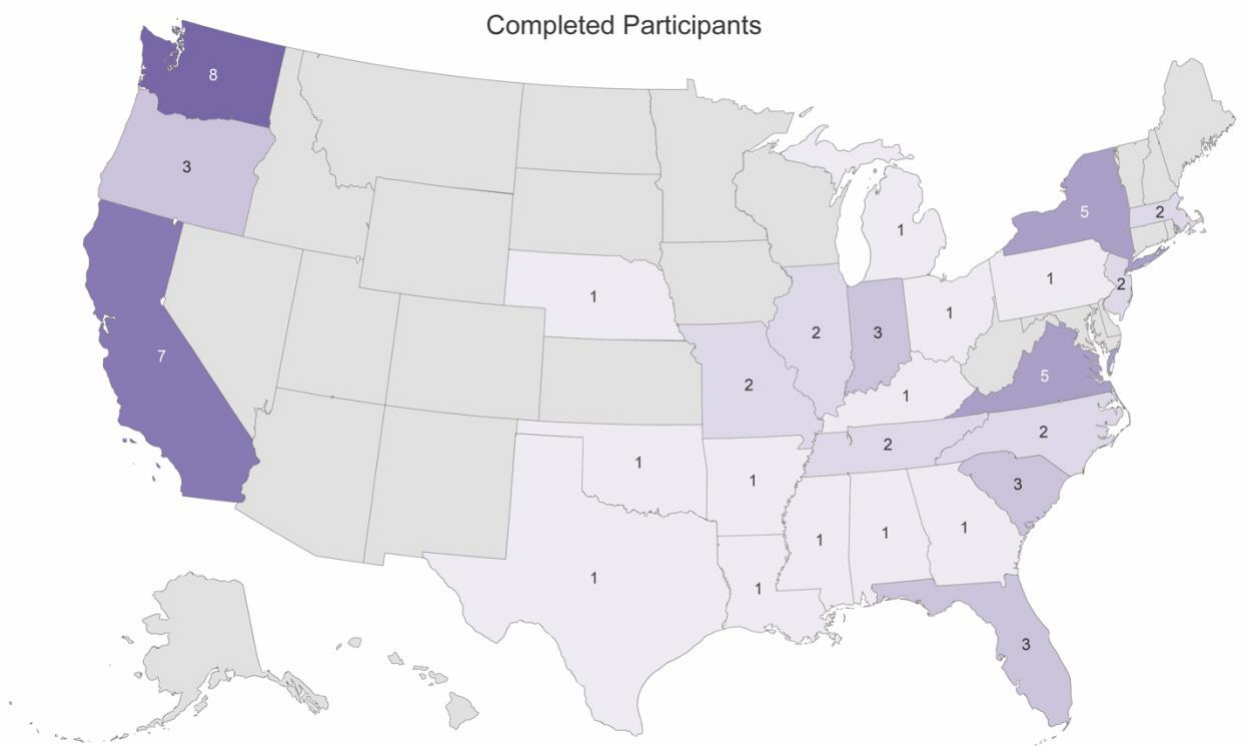

Figure 4.5. U.S. map of participants who have completed the study (n = 61).

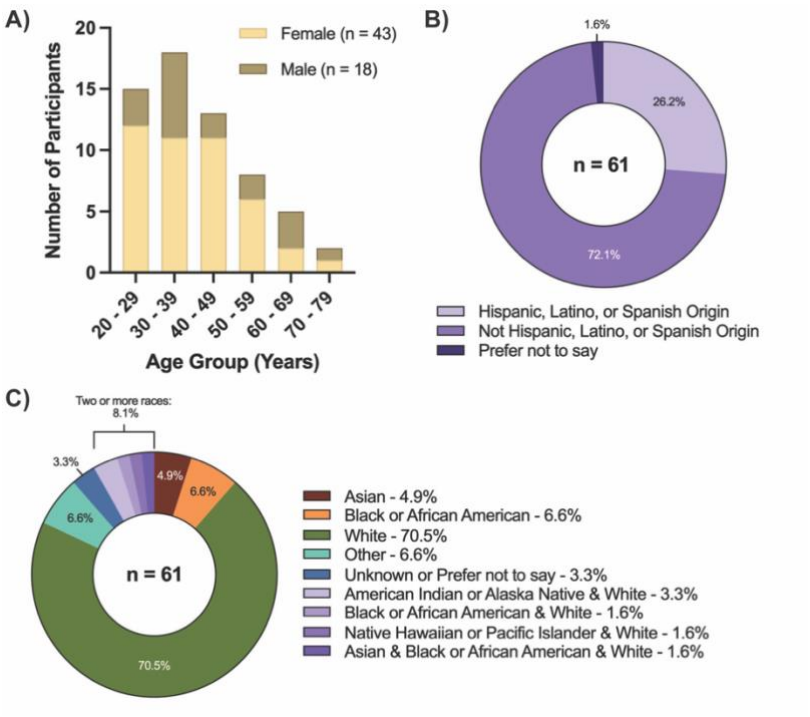

Figure 4.6. Demographic information for individuals who have completed the study. A) Age and sex demographics by age group. B) Ethnic demographics. C) Race demographics. (n = 61).

4.4 Kit Usability and Participant Response

As shown in Figure 1, participants collected blood and nasal samples each day for the first week, followed by one blood sample per week for days 14, 21, and 28. In addition to these sample collections, participants responded to daily surveys to help the study team track participant symptoms; these surveys also allowed participants to provide feedback on usability of the sample collection kits. Questions included usage time for the kit, pain levels, blood collection levels, and amount of time the Tasso-SST device remains on the participant's arm.

For nasal sample collection, 36 participants (59%) reported using less than 5 minutes for every sample they collected; for all nasal samples reported, 87% took less than 5 minutes to be collected (Figure 4.7A). Participants also reported on the amount of pain or discomfort experienced when

collecting the nasal sample (Figure 4.7B). 55 participants (90%) reported either no pain or mild pain or discomfort, and only 1 participant reported severe pain or discomfort.

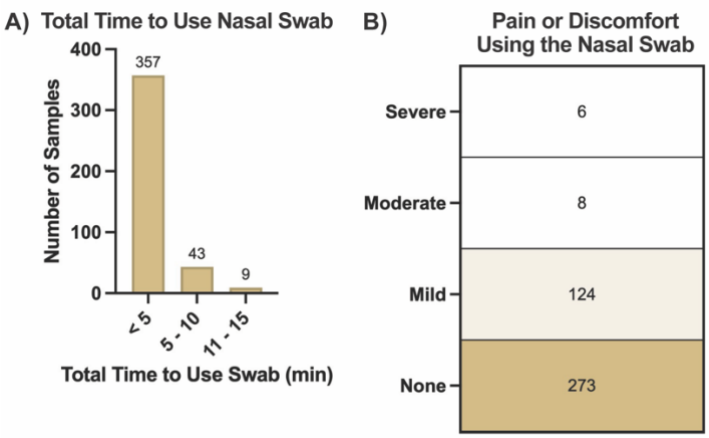

Figure 4.7. Nasal collection kit feedback. A) Amount of time used to obtain a nasal swab sample (n = 409). B) Pain or discomfort using the nasal swab (n = 411).

During blood sample collection participants were asked to report the amount of blood collected in reference to the image provided in Figure 4.8B. After blood collection participants transfer the blood to a stabilization tube. As seen in Figure 4.8A, participants reported varying amounts of blood collection; only 1% of sample collections failed to result in blood collected. Figure 4.8D shows the level of pain or discomfort participants experienced when using the Tasso-SST device. 60% of the blood collections resulted in no pain or discomfort, and only 8 participants (13%) reported moderate pain or discomfort during at least one blood collection.

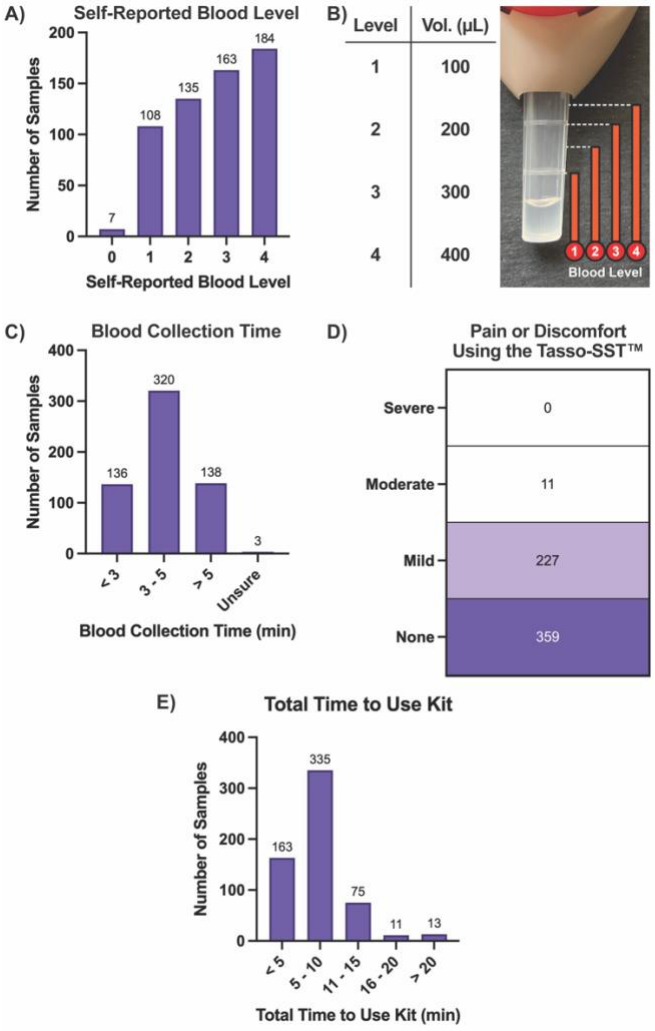

Figure 4.8. Blood collection kit feedback. A) Self-reported blood level, based on the image provided to participants shown in B. B) Blood collection levels in the Tasso-SST™ device and the corresponding volumes. C) Amount of time required for blood collection. D) Pain or discomfort levels when using the Tasso-SST™ device. E) Total time to use the *home*RNA kit. (n = 597).

As shown in Figure 4.7 and Figure 4.8, 87% of the nasal samples and 76% of the blood samples took less than 5 minutes to collect. The overall time needed to use the *home*RNA kit is shown in Figure 8E, showing that 83% of participants took up to 10 minutes in total to use the kit. Given the longitudinal nature of this study, requiring up to 28 days of participation and 10 total days of sampling, it is important that the total kit usage time is not a deterrent from participation. These

results are encouraging for potential future studies that also make use of the nasal sample collection kit and the *homeRNA* blood collection kit.

4.5 Conclusion and Moving Forward

Once the study is concluded, the nasal and blood samples will be analyzed in conjunction with the symptomatic data that participants reported. It is expected that some participants who were exposed to COVID-19 may not have contracted the virus and thus were neither symptomatic nor asymptomatic. The nasal samples will be analyzed for the presence of not only SARS-CoV-2 but also various other respiratory viruses such as influenza viruses, rhinoviruses, adenoviruses, and non-SARS coronaviruses. The blood samples will be analyzed for RNA yield and blood gene expression using the NanoString Host Response Panel with SARS-CoV-2 panel plus addition (NanoString, Seattle, WA). The protocols established in this study will be expanded in the future to study the immune response of viruses such as seasonal influenza viruses and other respiratory viruses.

4.6 References

1. A. J. Haack, F. Y. Lim, D. S. Kennedy, J. H. Day, K. N. Adams, J. J. Lee, E. Berthier, A. B. Theberge, "*home*RNA: A self-sampling kit for the collection of peripheral blood and stabilization of RNA." *Anal. Chem.*, 2021, **93**, 13196-203

Chapter 5. CONCLUSION

The topic of dissertation has covered open microfluidics, cell culture in three-dimensional structures, and an UW IRB-approved study involving the immune response to COVID-19. As discussed in Chapter 2, an open microfluidics system was designed to study the impact of combining capillary channels with paper pads on the velocity and flow rates of various liquids. In Chapter 3, two different methods of generating hydrogel lumens. The first method presented the casting of hydrogel rings out of collagen I hydrogel. This first method was analyzed for its ability to cast hydrogel rings reproducibly, the incorporation of smooth muscle cells within the hydrogel rings as well as the addition of endothelial cells to the lumen of the hydrogel rings, and finally showed the percent change in ring are when smooth muscle cell-laden hydrogel rings were treated with a vasodilator. The second method presented the fabrication of hydrogel tubes comprised of pluronic F127 and collagen I by extrusion through a coaxial nozzle. As shown in Chapter 3, while endothelial cells were unable to adhere to the pluronic F127 hydrogel, upon incorporation of collagen I the endothelial cells were successfully able to adhere and were cultured up to 72 h. Finally, in Chapter 4 the study design for the UW IRB-approved *STUDY00007868* was presented along with preliminary participant information as well as feedback regarding the study kit. At the time of this dissertation, the nasal swab and blood samples from study participants are still being analyzed.

VITA

Ashley M. Dostie has enjoyed her time at the University of Washington while pursuing her Ph.D. While attending the University of Washington, she has discovered her love of teaching while working with undergraduates in the general chemistry courses as a Teaching Assistant.